1995

An Observational Study of the "Interstate 5" Dust Storm Case

Pauley, Patricia M.

Bulletin of the American Meteorological Society, Vol. 77, No. 4, April 1996, pp. 693-720
http://hdl.handle.net/10945/40157

An Observational Study of the "Interstate 5" Dust Storm Case

Patricia M. Pauley,*+ Nancy L. Baker,# and Edward H. Barker#

ABSTRACT

On 29 November 1991 a series of collisions involving 164 vehicles occurred on Interstate 5 in the San Joaquin Valley in California in a dust storm that reduced the visibility to near zero. The accompanying high surface winds are hypothesized to result from intense upper-tropospheric downward motion that led to the formation of a strong upper front and tropopause fold and that transported high momentum air downward to midlevels where boundary layer processes could then mix it to the surface. The objectives of the research presented in this paper are to document the event, to provide support for the hypothesis that both upper-level and boundary layer processes were important, and to determine the structure of the mesoscale circulations in this case for future use in evaluating the navy's mesoscale data assimilation system.

The strong upper-level descent present in this case is consistent with what one would expect for jet streak and frontal circulations in combination with quasigeostrophic processes. During the period examined, upper-level data and analyses portray a strong upper-tropospheric jet streak with maximum winds initially in excess of 85 m s^{-1} (≈170 kt) that weakened as it propagated southward around the base of a long-wave trough. The jet streak was accompanied by a strong upper front and tropopause fold, both of which imply intense downward motion. The vertical motion field near the time of the accidents had two maxima—one that was associated with a combination of quasigeostrophic forcing and terrain-induced descent in the lee of the Sierra and one that was associated with the descending branch of the secondary circulation in the jet streak exit region and the cold advection by both the geostrophic wind and the ageostrophic wind in the upper front. The 700-hPa wind speed maximum over and west of the San Joaquin Valley overlapped with the latter maximum, supporting the hypothesized role of downward momentum transport.

Given the significant 700-hPa wind speeds over the San Joaquin Valley during daytime hours on the day of the collisions, boundary layer mixing associated with solar heating of the earth's surface was then able to generate high surface winds. Once the high surface winds began, a dust storm was inevitable, since winter rains had not yet started and soil conditions were drier than usual in this sixth consecutive drought year. Surface observations from a variety of sources depict blowing dust and high surface winds at numerous locations in the San Joaquin Valley, the Mojave and other desert sites, and in the Los Angeles Basin and other south coast sites. High surface winds and low visibilities began in the late morning at desert and valley sites and lasted until just after sunset, consistent with the hypothesized heating-induced mixing. The 0000 UTC soundings in California portrayed an adiabatic layer from the surface to at least 750 hPa, also supporting the existence of mixing. On the other hand, the high winds in the Los Angeles Basin began near sunset in the wake of a propagating mesoscale trough that appeared to have formed in the lee of the mountains that separate the Los Angeles Basin from the San Joaquin Valley.

1. Introduction

During the Thanksgiving weekend of 1991 strong surface winds along Interstate 5 (I-5) on the west side of California's San Joaquin Valley led to low visibility from blowing dust and contributed to the nation's worst multiple-vehicle collision to date (Fig. 1). According to a task force report (State of California 1992), 33 collisions occurred in a 2-mile (3.2 km) stretch of I-5 between 1330 and 1440 PST (2130 and 2240 UTC) 29 November approximately 40 miles (64 km) west of Fresno. The location of the accidents, indicated by the asterisk in Fig. 2, is in an agricultural region roughly halfway between San Francisco and Los Angeles (LA).

*Computer Sciences Corporation, Monterey, California
+Additional affiliation: Naval Postgraduate School, Monterey, California.
#Naval Research Laboratory, Monterey, California.
Corresponding author address: Prof. Patricia M. Pauley, Department of Meteorology, Naval Postgraduate School, Monterey, CA 93943-5114.
In final form 14 November 1995.

FIG. 1. Cleanup work on a portion of the accident site the day after the 29 November 1991 I-5 collisions. Thirty-three separate collisions involving 164 vehicles occurred on a 2-mile stretch of I-5 in a period of just over an hour in near-zero visibility resulting from blowing dust (AP/Wide World Photos).

At least 164 vehicles and 349 people were involved in the collisions, with 151 injured and 17 dead. Half of the 33 collisions and all of those involving fatalities occurred in the 6-min period from 1423 to 1429 PST. Fourteen of the collisions, involving 99 vehicles and 10 of the fatalities, took place on the southbound side of I-5, while the other 19 collisions were on the northbound side. That the most severe collisions occurred in the southbound lanes was attributed by the task force report (State of California 1992) to the fact that the vehicles in the southbound lanes were moving at an estimated average speed of 63 mph (101 km h^{-1}) prior to entering the dust storm, compared to those in the northbound lanes traveling at 48 mph (77 km h^{-1}). The greater speed in the southbound lanes was in turn attributed to the southbound drivers having driven through only small intermittent, though dense, clouds of dust north of the accident site, whereas the northbound drivers had encountered steadily decreasing visibility. The traffic on I-5 was also heavier and traveling faster than usual on this holiday weekend. In addition to the collisions at this primary site, another 30 collisions associated with blowing dust were reported on this day at locations in the southern San Joaquin Valley from Madera (30 km northwest of Fresno) to Bakersfield.

Although the San Joaquin Valley is a relatively dusty place, dust storms of the severity of this case are not common. The task force report on the collisions (State of California 1992) included a review of accident reports for the stretch of I-5 where the collisions occurred; it did not find any in the previous 10 years in which wind-blown dust was a factor. Using conventional surface hourly data, Orgill and Sehmel (1976) compiled a climatology of dust storms, which they defined as dust events reducing the visibility below 7 miles (11.3 km). Their results show that fall is the dustiest time of year in the San Joaquin Valley, but blowing dust sufficiently thick to reduce the visibility below their threshold is uncommon. The frequency of dusty hours in the valley is 0.6% in October, a local maximum but considerably smaller than the March maximum of 7% in west Texas. Even so, suspended dust is present often enough that the Environmental Protection Agency is proposing sanctions for San Joaquin Valley growers for not attaining the standard for particulate matter of 10 μm or greater (D. Gudgel 1995, personal communication).

Conditions in November 1991 paralleled the most important factors found by Pollard (1978) to be favorable for blowing dust in the southern Great Plains—proximity to a dust source, dry soils left unprotected, reduced plant cover associated with previous dry years, and winds in excess of 15 m s^{-1} (29 kt). First of all, this normally dry region was in its sixth

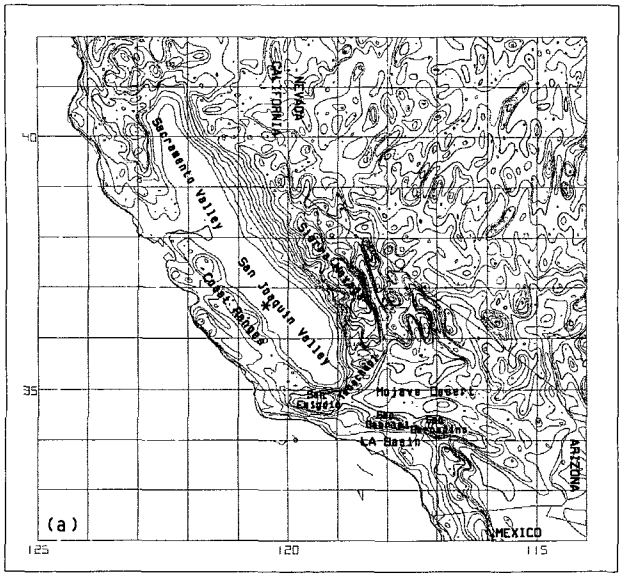

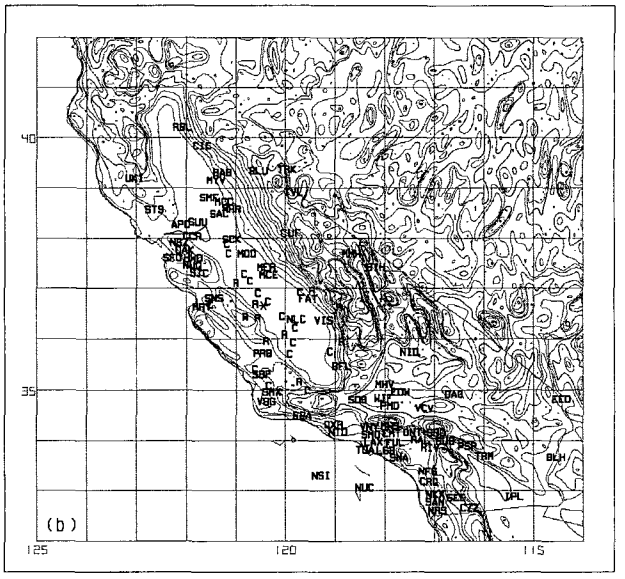

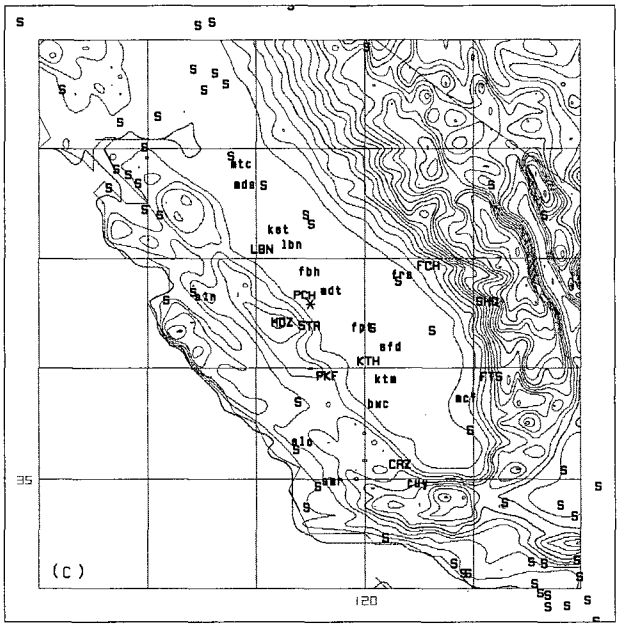

FIG. 2. Maps of California depicting topography and (a) geographical features or (b) locations of SA stations (three-letter identifiers), CIMIS stations ("C"), and RAWS stations ("R"). A close-up view of the San Joaquin Valley is shown in (c) with locations of SA stations ("S"), CIMIS stations (lowercase identifiers), and RAWS stations (uppercase identifiers). The location of the accident site is shown by the asterisk. Topography is contoured with a 200-m interval; bold contours are at 0, 1000, 2000, and 3000 m. The identifiers for Burbank (BUR), located just east of VNY, and Hawthorne (HHR), just east of LAX, were omitted to improve legibility.

and most severe year of drought (State of California 1992). Lemoore Naval Air Station, in the center of the San Joaquin Valley, had near-normal precipitation for calendar year 1991, but 6.06 in. (15.4 cm) of the 7.45-in. (18.9 cm) total fell in the first three months. Perhaps more importantly, the rainy season that normally begins in November had not yet begun by the Thanksgiving holiday. The only significant precipitation at Lemoore between 21 April and 6 December was 0.22 in. (0.56 cm) on 25–26 October. Second, the land north and east of I-5 at the site of the collisions had been declared fallow to the U.S. Department of Agriculture by the farmers, meaning that these fields were left unplanted after being plowed (State of California 1992). The plowing is noteworthy, since plowing or otherwise disturbing a soil surface makes it much more susceptible to dust generation (Gillette et al. 1980; Hall 1981; Nakata et al. 1981). In the San Joaquin Valley, in general, dust sources were abundant at this time for several reasons—less land under tillage because of limits on irrigation water, an early cotton harvest followed by plowing for pest control, and other areas with alkali soil that are unsuitable for agriculture but naturally dusty (D. Gudgel 1995, personal communication). Conditions were therefore ripe for a dust storm, lacking only high surface winds.

Previous studies of dust storms have found that the associated high surface winds result primarily from thunderstorms, frontal passages, or strong large-scale pressure gradients (e.g., Pollard 1978; Nickling and Brazel 1984). Thunderstorm-related dust events, such as the "haboob" discussed in Idso et al. (1972), are generated by the strong winds at and behind a gust front and typically last an hour or less (Nickling and Brazel 1984). Strong surface winds can also accom-

pany cold fronts, both at the front and extending well behind it (e.g., Bluestein 1993, 258, Fig. 2.18). In fact, Pollard (1978) cites cold fronts as the most frequent cause of widespread dust storms. Pollard (1978) and Nickling and Brazel (1984) also found dust events associated with features such as leeside troughs and extratropical cyclones, where large-scale pressure gradients and their implied geostrophic winds are strong. Although not mentioned explicitly in these two studies, local effects also contribute to high winds. The dust storms documented by Nakata et al. (1981) and Wilshire et al. (1981) in the Mojave Desert and southern San Joaquin Valley, respectively, occurred near steep orography under Santa Ana conditions, with winds locally accelerated by being funneled through canyons.

The event discussed in this paper, however, occurred in the absence of thunderstorms or a surface cold front, in a pressure gradient of only moderate intensity, and with orographic processes at best a secondary influence. The strong winds were all the more noteworthy given the weak winds expected in the Central Valley. For example, Lemoore Naval Air Station had a gust of 42 kt (21 m s^{-1}), compared to the mean wind speed for November of 5 kt (2.6 m s^{-1}), the record maximum gust for November of 45 kt (23 m s^{-1}), and the maximum gust for the entire 30-year record of 49 kt (25 m s^{-1}). As will be shown, conditions aloft were marked by a strong upper-level jet streak and upper front in highly amplified northwesterly flow present over the state of California. We hypothesize that the intense downward motion that led to the formation of the upper front and accompanying tropopause fold also transported high-momentum air downward to midlevels where boundary layer processes then mixed it to the surface, a mechanism similar to that described by Danielsen (1974, 1975).

The objectives of this research are to document the blowing dust event and its associated high surface winds, to provide support for the hypothesis that both upper-level and boundary layer processes were important in generating high surface winds, and to determine the structure of the mesoscale circulations present in this case for use in a future evaluation of the navy's mesoscale data assimilation system. To better portray conditions in the data-sparse San Joaquin Valley, additional surface data, low-level aircraft soundings, and automated aircraft observations were obtained to supplement conventional surface airways and rawinsonde reports. The characteristics of these data are discussed in the following section. A synthesis of the surface observations is then given to examine the temporal and spatial extent of the blowing dust and high surface winds. Surface analyses are presented to further investigate the spatial distribution of high winds and the role of surface troughs. Finally, conditions aloft and their relationship to the high surface winds are presented.

2. Data

Surface airways (SA) stations (indicated by identifiers in Fig. 2b and by the letter S in Fig. 2c) are relatively sparse in the San Joaquin Valley. Therefore, additional surface observations were obtained to enable a more complete depiction of meteorological conditions. Since SA reports are taken at airports, their distribution reflects the population distribution in California, with clusters of stations in the heavily populated San Francisco and Los Angeles metropolitan areas and widely separated stations elsewhere. The stations in the San Joaquin Valley tend to lie near or to the east of the center of the valley, mostly along California Highway 99.

The California Department of Water Resources operates the California Irrigation Management Information System (CIMIS), a network of approximately 80 automated weather stations. This network was established to aid in scheduling irrigation and therefore measures quantities different from the SA network, namely, hourly averages of solar radiation, soil temperature, air temperature, relative humidity, wind speed and direction (at 2 m), and precipitation. Data were obtained for 16 of these stations (indicated by "C" in Fig. 2b and by lowercase identifiers in Fig. 2c), mostly in agricultural areas near the center of the San Joaquin Valley.

Observations are also taken by Remote Automated Weather Stations (RAWS), operated by the California Department of Forestry and Fire Protection or the Bureau of Land Management. These stations aid in fire hazard and fire weather forecasting and measure hourly instantaneous values of barometric pressure, air temperature, relative humidity, peak wind gust and direction, fuel temperature, fuel moisture, and precipitation. The reported wind speed and direction are 10-min averages at a height of 20 ft (6.1 m). Data were obtained for 10 of these stations, primarily at middle to higher elevations in the foothills on either side of the San Joaquin Valley (indicated by the letter R in Fig. 2b and by uppercase identifiers in Fig. 2c).

These surface data were used with only minimal manipulation. All data were converted to meter, kilogram, second units, and dewpoint temperatures were computed from the available humidity data. To facilitate comparison with surface winds from other sources, CIMIS winds were extrapolated from 2 m to the standard anemometer height of 10 m by multiplying them by 1.3. This factor was obtained by assuming a logarithmic wind profile with a roughness length of 1 cm, appropriate for a neutral lapse rate overlying a grassy surface (e.g., Holton 1979, 106–107).

Low-level aircraft soundings are taken at a number of locations under contract to the California Air Resources Board. On 29 and 30 November 1991 soundings were available for Ukiah (UKI), Red Bluff (RBL), Chico (CIC), Sacramento (SAC), Columbia (CUF), Fresno (FAT), and Bakersfield (BFL) (Fig. 2b). The aircraft take temperature readings every 500 ft (150 m) from the surface to 5000 ft (1500 m) above ground level (AGL) sometime between 0300 and 0500 PST (1100 to 1300 UTC). Of special interest to this study was a second sounding taken at Sacramento (SAC) on 29 November at 1105 PST (1905 UTC). Pressures at the observed pressure altitudes were estimated for these soundings from the hypsometric equation assuming U.S. Standard Atmosphere temperatures, consistent with pressure altimetry (Hess 1959, 86). The pressure values and the observed temperatures were then used to compute potential temperatures.

ACARS [ARINC (Aeronautical Radio, Inc.) Communications, Addressing and Reporting System] wind observations are taken automatically every 7.5 min on many domestic jets (Benjamin et al. 1991). These data have the same availability as scheduled airline flights; the number of reports for this case over the western states (the area shown in Figs. 14–17) in a 6-h window centered on the given time varies from 54 at 1200 UTC to 640 at 1800 UTC on 29 November 1991, with 529 reports at 0000 UTC and 348 reports at 0600 UTC on 30 November. Most observations are taken at lower-stratospheric cruising altitudes; other levels are sampled as the aircraft ascends after takeoff or descends prior to landing.

Finally, the upper-air observations are plotted on analyses from the NORAPS (Navy Operational Regional Atmospheric Prediction System) mesoscale data assimilation system, run in research mode. The analyses presented in this paper used a 60-km mesh length in a 6-h update cycle, with the model run on 36 sigma levels and an optimum interpolation analysis performed on standard pressure levels (Hodur 1987; Barker 1992; Liou et al. 1994). Assimilated data included ACARS aircraft winds as well as observations from the navy's operational database (Baker 1992), which include surface data (land and marine), upper-air data (rawinsonde and PIBAL), and conventional aircraft reports, as well as satellite-derived cloud-tracked winds, surface wind speeds, and temperature soundings.

3. Extent of blowing dust conditions

Determining the details of the spatial and temporal extent of this blowing dust (BD) event is not straightforward, since visibility is measured only at SA stations and the cause of visibility reductions is given only at SA stations that are manned. Given the incomplete coverage of the San Joaquin Valley by the SA stations, their direct observations of BD are supplemented by indirect observations using satellite imagery and solar radiation measurements at CIMIS stations. This section discusses the observations of the blowing dust event and its accompanying strong winds and examines them for evidence of the hypothesized role of boundary layer mixing.

During the 24-h period beginning at 1200 UTC 29 November 1991, a total of 123 SA reports were found for California in which BD was either observed as current weather or noted in the comments. A few reports of haze or obscured sky were included when they directly preceded or followed BD reports and so were judged to be related to the BD event. Table 1, which summarizes these observations, shows that blowing dust was quite widespread. Reports occurred not only in the San Joaquin Valley but also in the Salinas Valley [which extends southeast from Salinas (SNS) to Paso Robles (PRB)], in desert locations in southeastern California, and along the South Coast from Santa Maria (SMX) to Santa Ana (SNA) (Fig. 2).

Lemoore Naval Air Station (NLC), the SA station closest to the accident site, had arguably the worst conditions of the SA stations during this 24-h period, reporting visibility less than 1 km for at least 2 h (Fig. 3a).[1] The period of reduced visibilities, obscured skies,

[1]The missing observations at 1900 and 2100 UTC make it difficult to determine the actual beginning of the blowing dust event at NLC. However, the 1955 UTC observation was likely near the beginning, since it reports an obscured sky but no decrease in visibility.

TABLE 1. Summary of blowing dust observations in California from the SA dataset between 1200 UTC 29 November and 1200 UTC 30 November 1991.

Station		Duration (UTC)	Minimum visibility (km)	Mean hourly wind speed ($m\ s^{-1}$)	Maximum wind gust ($m\ s^{-1}$)
San Joaquin Valley					
SCK	Stockton	1854–2153	24.0	13.3	19.6
MER	Castle AFB	1855–2055	4.8	11.2	17.0
MCE	Merced	2045–2252	6.4	7.7	14.4
NLC	Lemoore NAS	1955–0155	0.5	12.5	21.6
BFL	Bakersfield	1950–2354	3.2	10.7	17.5
Salinas Valley					
PRB	Paso Robles	2045–2154, 2350	0.8	14.4	21.6
South Coast					
SMX	Santa Maria	2150, 0050	24.0	9.0	16.0
SBA	Santa Barbara	0048, 0248, 0451, 0558	8.0	9.1	13.4
OXR	Oxnard	0018–0446*	2.4	7.5	
NTD	Point Mugu NAS	0040–0855	1.6	7.4	10.3#
VNY	Van Nuys	2331–0246	1.2	12.1	28.3
BUR	Burbank	2346–0105	3.2	9.0	15.5
SMO	Santa Monica	2346–0246	1.6	9.9	23.2
LAX	Los Angeles	0051–0150	4.8	10.8	16.0
HHR	Hawthorne	0046–0151	3.2	10.3	15.5
FUL	Fullerton	0150	8.0	10.3	
TOA	Torrance	0046–0151	4.8	9.8	18.0
LGB	Long Beach	0050–0150	6.4	10.6	13.9
SNA	Santa Ana/Orange	0150–0246	8.0	7.7	
Southeast Desert					
MHV	Mojave	1703–1850*	0.0	24.5	33.5
EDW	Edwards AFB	1655–2355	16.0	13.7	15.5
WJF	Lancaster	1646–2356, 0346	16.0	11.9	16.5
PMD	Palmdale	1852–0046	8.0	11.3	19.1
DAG	Daggett	1950–2018	0.8	14.4	21.6
IPL	Imperial	2230–2350	6.4	13.1	21.6
BLH	Blythe	1950–2350	3.2	9.1	11.3

*Blowing dust may have lasted longer; some reports were missing.

#While NTD reported a maximum gust of only 10.3 $m\ s^{-1}$ during the period of BD, the remarks at 0155 UTC gave a wind gust of 28.8 $m\ s^{-1}$ at Laguna Peak, approximately 4 km to the east.

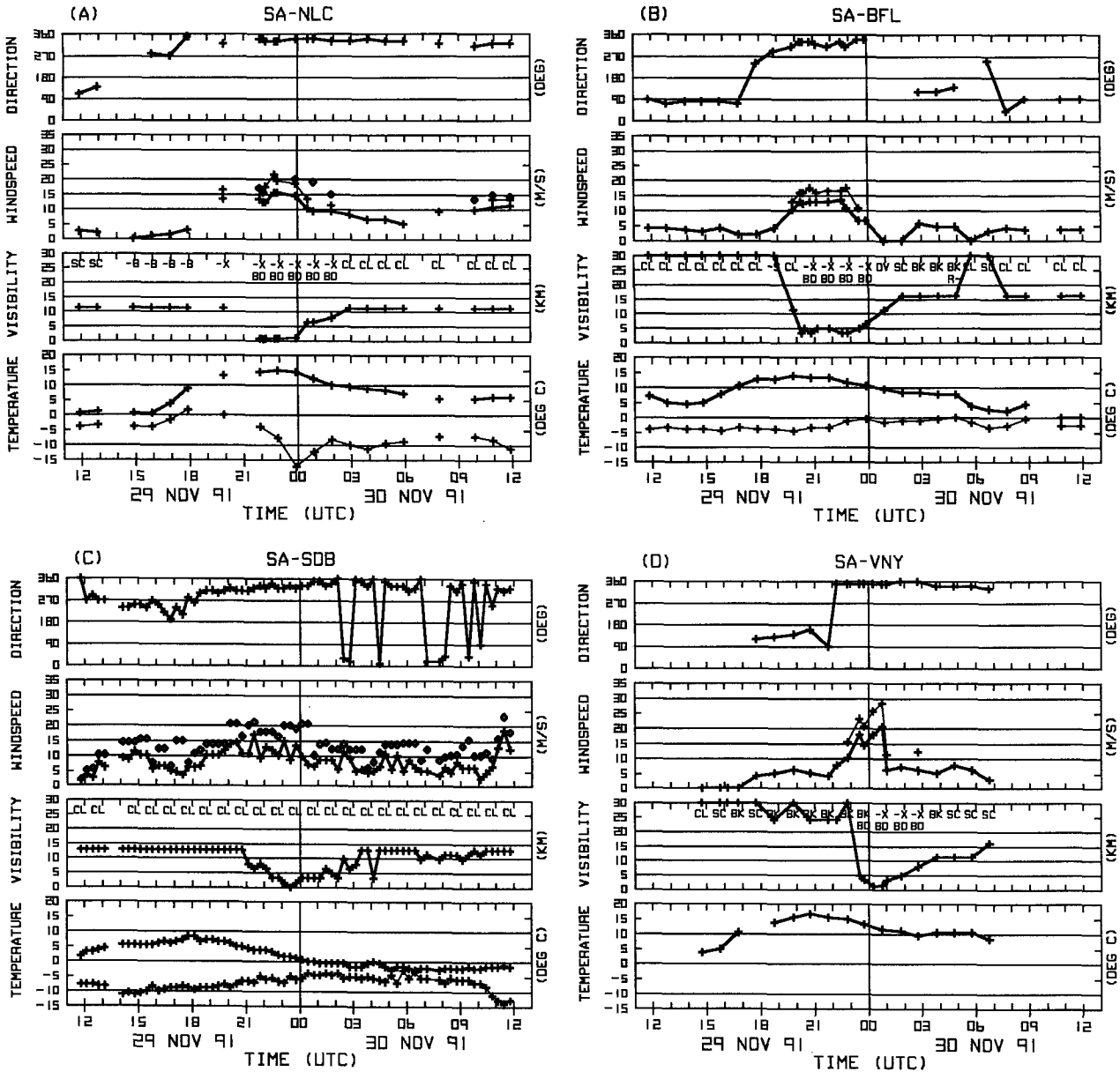

FIG. 3. Meteorograms from the SA dataset for (a) NLC, (b) BFL, (c) SDB, and (d) VNY. From top to bottom, quantities plotted include wind direction (degrees); wind speed (bold line, m s^{-1}), gust speed (thin line, m s^{-1}), and peak wind speed (diamond symbol, m s^{-1}); visibility (km), sky cover (top line), and observed weather (bottom line); and temperature (bold line, °C) and dewpoint temperature (thin line, °C). The sky cover is abbreviated CL for clear, SC for scattered, BK for broken, –B for thin broken, OV for overcast, and –X for thin obscured. Note that Sandburg, an automated station, did not report observed weather but blowing dust was inferred from the reduced visibility that began at 2100 UTC.

and reported BD corresponds very well with the period of strong winds. In addition, the dewpoint temperature plummeted from 0° to –17°C during this period, consistent with the hypothesized mixing of boundary layer air with drier air aloft. Temperatures at NLC were dominated by diurnal changes and show no evidence of a frontal passage.

However, the BD at NLC was in some respects unrelated to the BD at the accident site. Figure 4 shows an enhanced AVHRR (Advanced Very High Resolution Radiometer) satellite image at 2204 UTC, approximately a half hour before the accidents. This image portrays a narrow dust plume near the center of the San Joaquin Valley passing through NLC. A

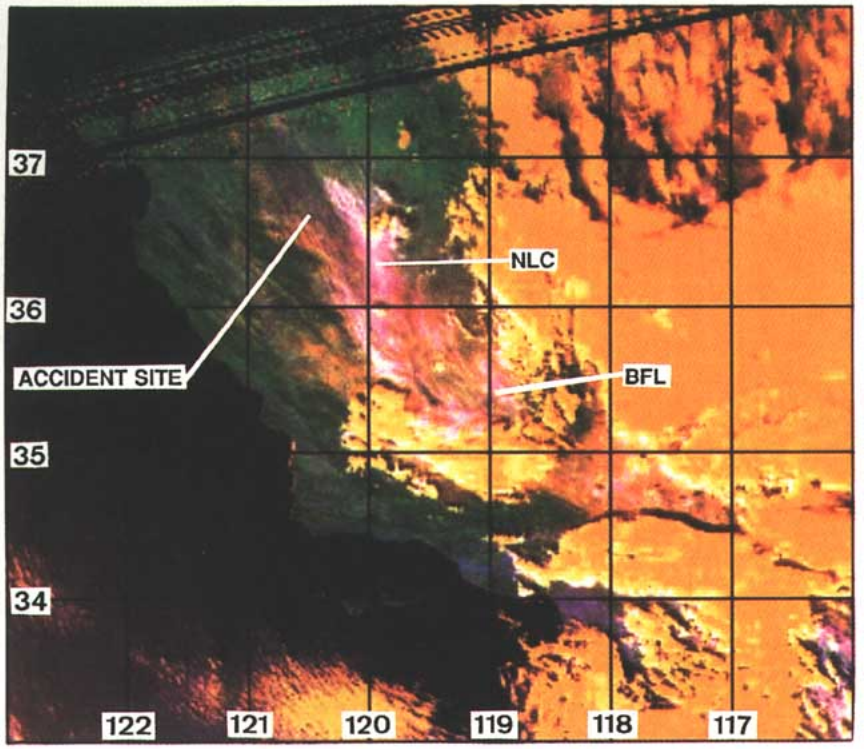

FIG. 4. Enhanced AVHRR image for 2204 UTC 29 November 1991. Channels 1 (0.63 μm visible), 2 (0.87 μm visible), and 3 (3.7 μm near-infrared) were mapped as red, green, and blue, respectively, and enhanced individually using a piecewise linear technique to bring out detail in the dust plumes in the San Joaquin Valley at the expense of detail in the cloud tops. As a result, the dust appears as shades of magenta and clouds appear yellow. Latitude and longitude lines are drawn using a 1° interval to facilitate comparison with the geography portrayed in Fig. 2.

separate dust plume is present along the western edge of the valley at and south of the accident site, with more dust in the southern part of the valley near Bakersfield and in the Mojave Desert east of Sandburg. Animations of high-resolution Geostationary Operational Environmental Satellite (GOES) visible imagery (not shown) confirm the southeastward advection of dust in two distinct plumes in the San Joaquin Valley. The existence of multiple plumes most likely reflects the distribution of dust sources, as found by Nakata et al. (1981) for six Mojave Desert dust plumes. In addition, the satellite imagery shows a near absence of clouds over the valley, ruling out the influence of a thunderstorm gust front in generating the high winds.

The solar radiation observations in the CIMIS dataset also provide evidence for two distinct dust plumes. Table 2 includes those locations where the suspended dust was sufficiently optically thick to reduce the hourly average solar radiation by at least 50 W m^{-2} relative to unrestricted conditions. (The unrestricted value was estimated as the maximum hourly average solar radiation for the same hour from the period 27 November to 1 December 1991, while the 50 W m^{-2} criterion represents approximately 10% of the noontime hourly average solar radiation.) Mendota (mdt) was the station closest to the accident site but was just west of the dust plume that affected NLC and east of the plume affecting the accident site; it therefore had only a minimal reduction in solar radiation (Fig. 5a). Stratford (sfd), on the other hand, was affected by the same dust plume as NLC and had up to a 60% reduction in solar radiation as well as a sharp decrease in dewpoint temperature similar to that at NLC (Fig. 5b).

One of the more interesting aspects of this case is its timing; the observations of BD at SA stations in the San Joaquin and Salinas Valleys and in the southeast desert occurred primarily before 0000 UTC, while the south coast reports occurred primarily after 0000 UTC (Fig. 6). The former reports began near the time of peak insolation (2000 UTC), as expected if boundary layer heating and mixing were important. The blowing dust along the south coast, however, occurred too close to sunset (0100 UTC) for boundary layer heating to be a dominant factor.

The meteorograms in Fig. 3 portray this nearly simultaneous initiation of BD at valley and desert stations. The onset of BD, low visibilities, and high wind speeds at BFL (Fig. 3b) occurs at 1950 UTC, very nearly the same time as at NLC 130 km to the northwest. Similar timing in the onset of low visibilities and high wind speeds is also apparent at the automated station at Sandburg (SDB), 80 km south-southeast of Bakersfield across the Tehachapi Mountains (Fig. 3c). The first report of strong winds at SDB was at 2008 UTC, with lowered visibility reported 1 h later.

TABLE 2. Summary of significant reductions in hourly average solar radiation at CIMIS stations in the San Joaquin Valley between 1800 UTC 29 November and 0000 UTC 30 November 1991. Only reductions greater than 50 W m^{-2} are included, with the exception of Firebaugh, a station close to the site of the accidents. The percentage reduction is defined as the ratio of the maximum reduction to the unrestricted value for that time. Hourly wind speeds have been adjusted to a height of 10 m assuming a logarithmic wind profile. Station identifiers correspond to those in Fig. 2c.

Station		Duration of 50 W m^{-2} reduction* (UTC)	Time of maximum reduction* (UTC)	Maximum reduction in solar radiation (W m^{-2})	Percent reduction	Hourly mean wind at maximum reduction	
						Direction	Speed (m s^{-1})
frs	Fresno State	2200	2200	58	15	11°	8.5
fbh	Firebaugh	—	2200	41	10	336°	15.0
mdt	Mendota	2200	2200	56	20	326°	17.5
fpt	Five Points	2000–2300	2200	73	17	339°	15.4
sfd	Stratford	2000–0000	2300	178	60	324°	14.8
ktm	Kettleman	2100–2200	2100	196	38	349°	14.6
bwc	Blackwells Corner	2200–0000	2200	246	62	345°	9.4
mcf	McFarland	2200–2300	2200	134	30	313°	9.1

*Data are averaged over the hour prior to the time reported.

The similarities in timing extend to the temperature field as well. Figure 7a portrays the temporal distribution of temperature at SA stations extending from RBL on the northern end of the Sacramento Valley to BFL on the southern end of the San Joaquin Valley (Fig. 2b). Little variation is present along the Cen-

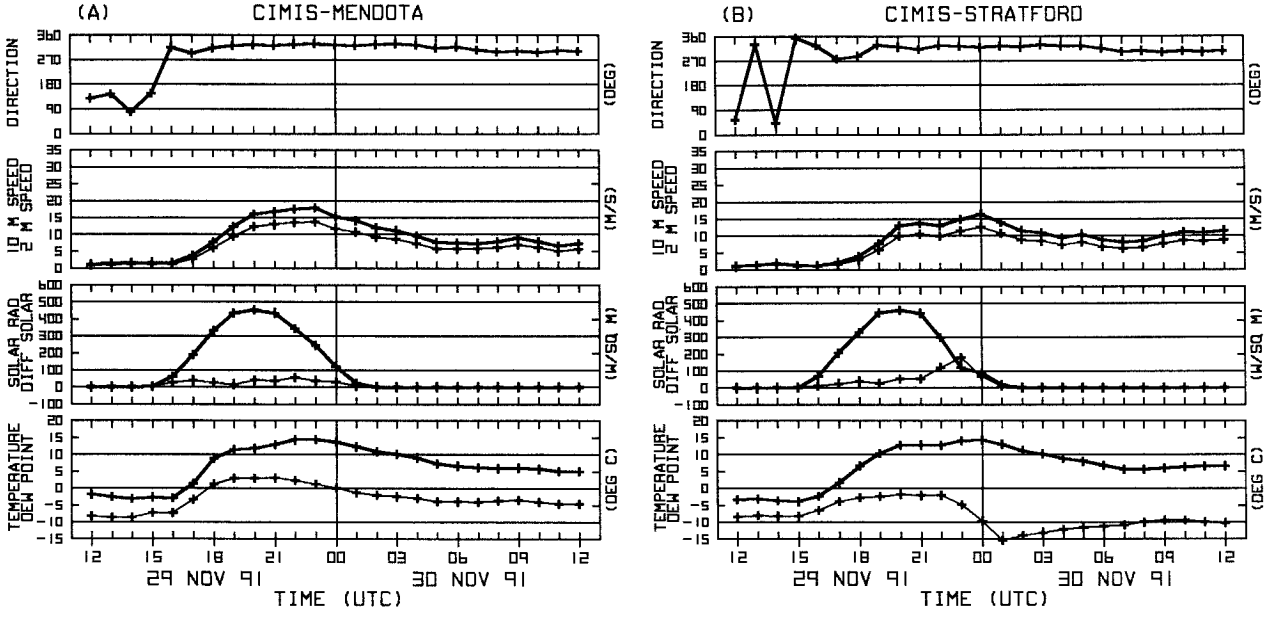

FIG. 5. Meteorograms from the CIMIS dataset for (a) mdt and (b) sfd. From top to bottom, quantities plotted include wind direction (degrees); wind speed extrapolated to 10 m (bold line, m s^{-1}) and wind speed observed at 2 m (thin line, m s^{-1}); solar radiation (bold line, W m^{-2}) and departure of observed solar radiation from estimated unrestricted values (thin line, W m^{-2}); and temperature (bold line, °C) and dewpoint temperature (thin line, °C). All quantities were averaged over the hour prior to the reported time. Unrestricted solar radiation was estimated as the maximum hourly average value for a given hour from the period 27 November to 1 December 1991. A positive solar radiation departure implies a reduction compared to unrestricted values.

tral Valley as temperatures rebound from the early morning near-freezing values. Even the midafternoon temperature maxima vary by only 3°C at all but Visalia (VIS) and BFL, the latter of which had clouds present in the late afternoon and evening (Fig. 3b). The highest wind speeds occur during the warmest part of the day, as would result from boundary layer mixing induced by surface heating. No evidence is seen to support a propagating feature such as a surface front.

The dewpoint temperatures, however, tell a different story (Fig. 7b). At most stations, the dew points increase to a midmorning maximum and then decrease rather abruptly. The decrease has a considerable variation in time, occurring earliest to the north (e.g., between 1800 and 2000 UTC at MYV) and progressively later to the south (e.g., between 0100 and 0300 UTC at VIS). The northern stations begin the strongest dewpoint decrease right at the onset of high winds, while the southern stations experience a several-hour delay between the onset of high winds and the beginning of the strongest dewpoint decrease. At a given time, therefore, the region experiencing a strong dewpoint decrease is relatively small. The magnitude of the decrease and its limited spatial extent are similar to the sudden mesoscale drying event discussed by Fuelberg et al. (1991), in which mixing induced by surface heating accessed a narrow tongue of dry midtropospheric air and yielded large decreases in surface dewpoint temperature over a small region. In the present case, the data are consistent with the southward propagation of a narrow dry tongue aloft, such as might occur in association with the hypothesized upper front.

While the observations in the Central Valley are consistent with the hypothesized boundary layer mixing and rule out a propagating feature at the

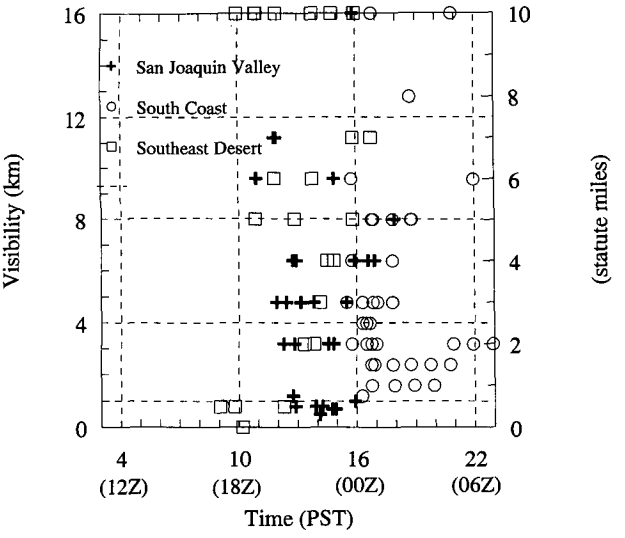

FIG. 6. Visibility (km) as a function of time (PST) for SA stations reporting blowing dust in the San Joaquin and Salinas Valleys (+), the south coast including the LA Basin (○), and in the southeast desert including the Mojave (□). Equivalent UTC times are given along the abscissa in parentheses. The *y* axis is also labeled in statute miles, the unit used in the original observations.

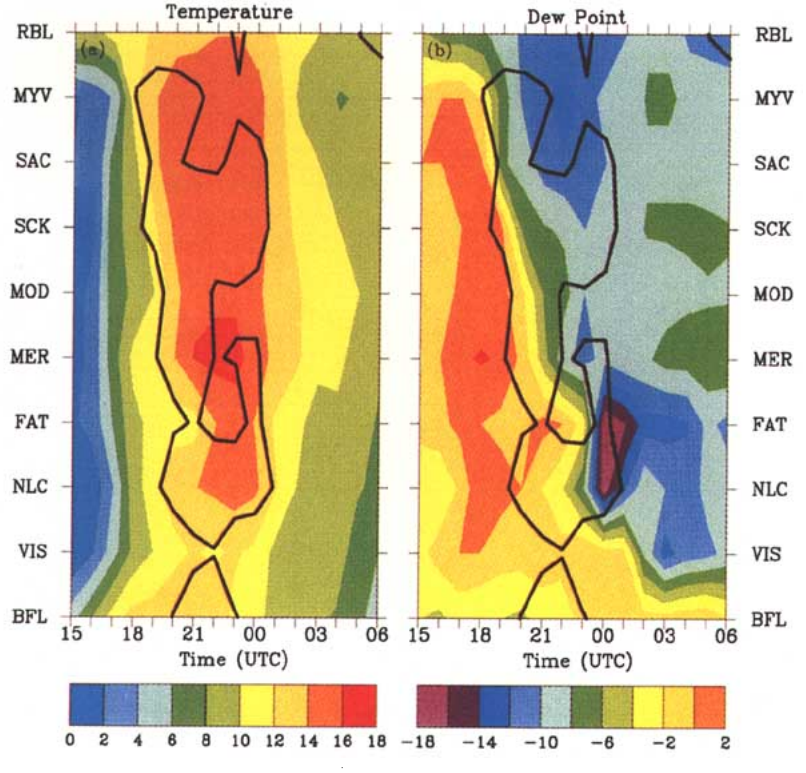

FIG. 7. (a) Temperature (°C) and dewpoint temperature (°C) as a function of time and space for SA stations along the Sacramento and San Joaquin Valleys from north (top) to south (bottom). The stations include RBL, Marysville (MYV), SAC, Stockton (SCK), Modesto (MOD), Merced (MER), FAT, NLC, VIS, and BFL. Station locations are given in Fig. 2b. The 10 m s^{-1} isotach is also plotted as a bold black line, with speeds higher than 10 m s^{-1} occurring roughly between 2000 and 0100 UTC. Note that the variation in temperature is primarily diurnal, while the strong decrease in dewpoint temperature propagates along the Central Valley from north to south.

surface, the data for Van Nuys (VNY) at the northern edge of the Los Angeles Basin show strong gusty winds beginning later (at 2250 UTC compared to 1950 UTC), lasting a shorter period (2 h compared to 4–5 h), and accompanied by a more abrupt wind shift (Fig. 3d). The wind shift occurred at VNY and nearby Burbank (BUR) by 2250 UTC, at Los Angeles (LAX) and Long Beach (LGB) by 2350, and at SNA by 0150 UTC (see Fig. 2b for locations). These data suggest that the high winds were associated with a surface feature propagating through the LA Basin, a possibility that will be explored more fully in the next section.

Since surface wind speeds play such a crucial role in BD events, mean wind speeds and maximum gusts are summarized in Table 1 for the period in which BD was reported. The mean wind speed here is defined as the average of the hourly ("SA" or "RS") values during the period shown, with special ("SP") reports excluded. For the most part, the average values are well below the 15 m s^{-1} criterion for dust generation cited by Pollard (1978). However, these values are consistent with the mean wind speeds for Arizona dust storms given by Hall (1981) and Nickling and Brazel (1984). An examination of the most severe BD reports—those with visibilities less than or equal to 1 km—shows that they occurred with observed winds of 12.4–25.8 m s^{-1} and gusts of 15.4 to 30.9 m s^{-1} (Fig. 8), much more in line with Pollard's 15 m s^{-1} criterion. These extremely low visibilities and high wind speeds likely occurred in close proximity to regions of dust generation. Higher visibilities and lower wind speeds, on the other hand, imply the advection of already suspended dust, consistent with Pollard's criterion of wind speeds greater than or equal to 5 m s^{-1} (10 kt) for dust advection.

The cluster of south coast reports in Fig. 8a with visibilities less than 4 km and wind speeds less than 10 m s^{-1} seems to provide the exception to this rule but is more likely a consequence of station location in the highly variable terrain. Table 1 shows that Point Mugu Naval Air Station (NTD) had a minimum visibility of 1.6 km with a maximum gust of only 10.3 m s^{-1} during the period of BD. However, the remarks section of the 0155 UTC observation for NTD reported a gust of 28.8 m s^{-1} at Laguna Peak (approximately 4 km east of NTD), the highest gust reported on the south coast.

The complexity of the terrain also plays a role in yielding higher wind speeds and gusts in the RAWS dataset compared to the SA or CIMIS datasets. Figure 9 portrays wind speed and maximum gust for three of the RAWS stations along the western edge of the San Joaquin Valley. The Panoche Road station (PCH) is close to I-5 northwest of the accident site at an elevation of 152 m, compared to 57 m at the Mendota CIMIS station less than 30 km to the northeast on the

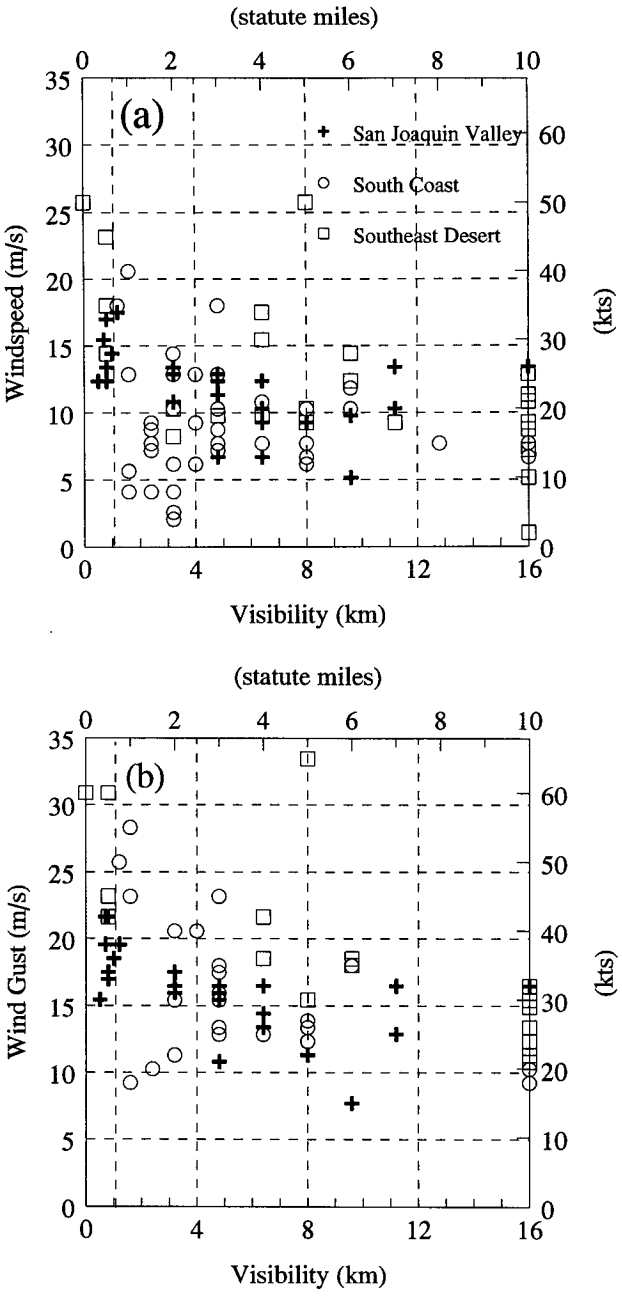

FIG. 8. (a) Wind speed (m s^{-1}) and (b) wind gust (m s^{-1}) as a function of visibility (km) for SA stations reporting blowing dust. Symbols are the same as in Fig. 3. The axes are also labeled in knots (right) and statute miles (top), the units used in the original observations.

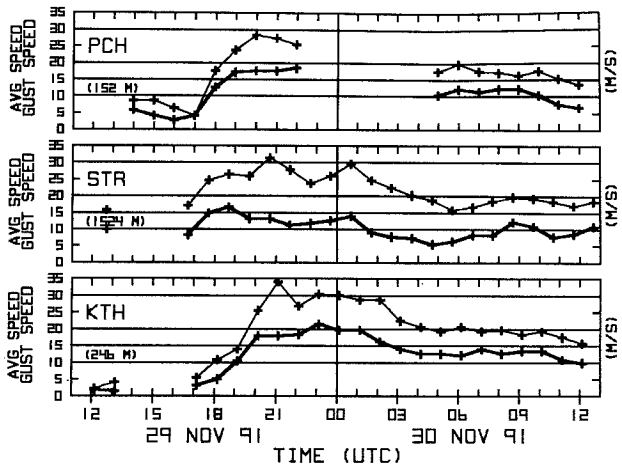

FIG. 9. Wind speed and peak gust speed from the RAWS dataset for Panoche Road (PCH), Santa Rita (STR), and Kettleman Hills (KTH). The reported wind speed is a 10-min average. Station elevations are listed on the plot in parentheses.

valley floor. A small side valley leads southwest into the mountains just west of PCH. The Santa Rita station (STR), south of the accident site at 1524 m, is located in a saddle north of a high peak with valleys to the east and west. Yet farther south, the Kettleman Hills station (KTH) is located on a hilltop at 246 m compared to 104 m at the Kettleman CIMIS station.

Winds at PCH and KTH increased in speed rapidly after 1700 UTC to sustained values greater than 15 m s^{-1} and maximum gusts of 28 and 34 m s^{-1}, respectively. STR had more modest sustained winds but gusts in excess of 20 m s^{-1} throughout the day and evening, likely related to its higher elevation. Wind directions (not shown) were northeasterly at PCH after 1800 UTC but northwesterly at the other two stations in agreement with the SA and CIMIS data. The northeasterly direction at PCH appears anomalous but is consistent with flow up the nearby side valley and with reports of easterly winds at the accident site by some of the drivers involved in the collisions and by the crew of a California Highway Patrol helicopter responding to the collisions (State of California 1992). The easterly component blowing across the interstate from the adjacent dry fields likely made visibility worse at the accident site than a northwesterly wind oriented along the interstate would have.

The implied up-valley flow at the accident site and the widespread nature of the strong northwesterly surface winds suggest that topographic effects are at best a secondary factor in generating the high surface wind speeds in this case, at least in terms of directly funneling the wind through gaps or canyons. In contrast, the December 1977 dust storm near Bakersfield described by Wilshire et al. (1981) had southeasterly surface geostrophic flow with the strongest observed winds at the base of the downwind side of mountains on the southern and eastern walls of the San Joaquin Valley where the flow was channeled through canyons.

In summary, surface data depict a widespread blowing dust event in predominantly northwesterly flow, with reports of BD or reduced solar radiation occurring in the San Joaquin and Salinas Valleys, the Mojave and other desert locations, and the LA Basin and other south coast locations. The data show that BD and high winds at valley and desert sites began nearly simultaneously at or just before local noon (2000 UTC) and ended at or just after local sunset (0100 UTC), consistent with the hypothesized role of daytime boundary layer mixing. On the other hand, the onset of BD and high winds at south coast stations began near sunset, were relatively short lived, and were not synchronized but rather seem to have been associated with a propagating feature. The role of propagating troughs is explored in more detail in the following section.

4. Low-level synoptic conditions

The high winds and accompanying blowing dust in California on 29 November 1991 occurred in a strengthening northwest–southeast pressure gradient between a strong quasi-stationary eastern Pacific anticyclone and an incipient low in southern California. The objectives of this section are to document any troughs and wind shifts that played a role in the blowing dust event and to further examine the role of boundary layer mixing. Manual analyses for California and surrounding states were prepared in order to examine the surface patterns for the period 1200 UTC 29 November to 0600 UTC 30 November in more detail than provided by operational analyses (not shown) from the National Meteorological Center (NMC, renamed the National Centers for Environmental Prediction). Figure 10 includes analyses for 1200 UTC 29 November, referred to as the "predawn" time since it is 0400 PST; 1800 UTC 29 November, referred to as the "pre-BD" time since it is just before BD reports began at valley and desert stations; 0000 UTC 30 November, referred to as the "near-sunset" time since sunset was between 0030 and

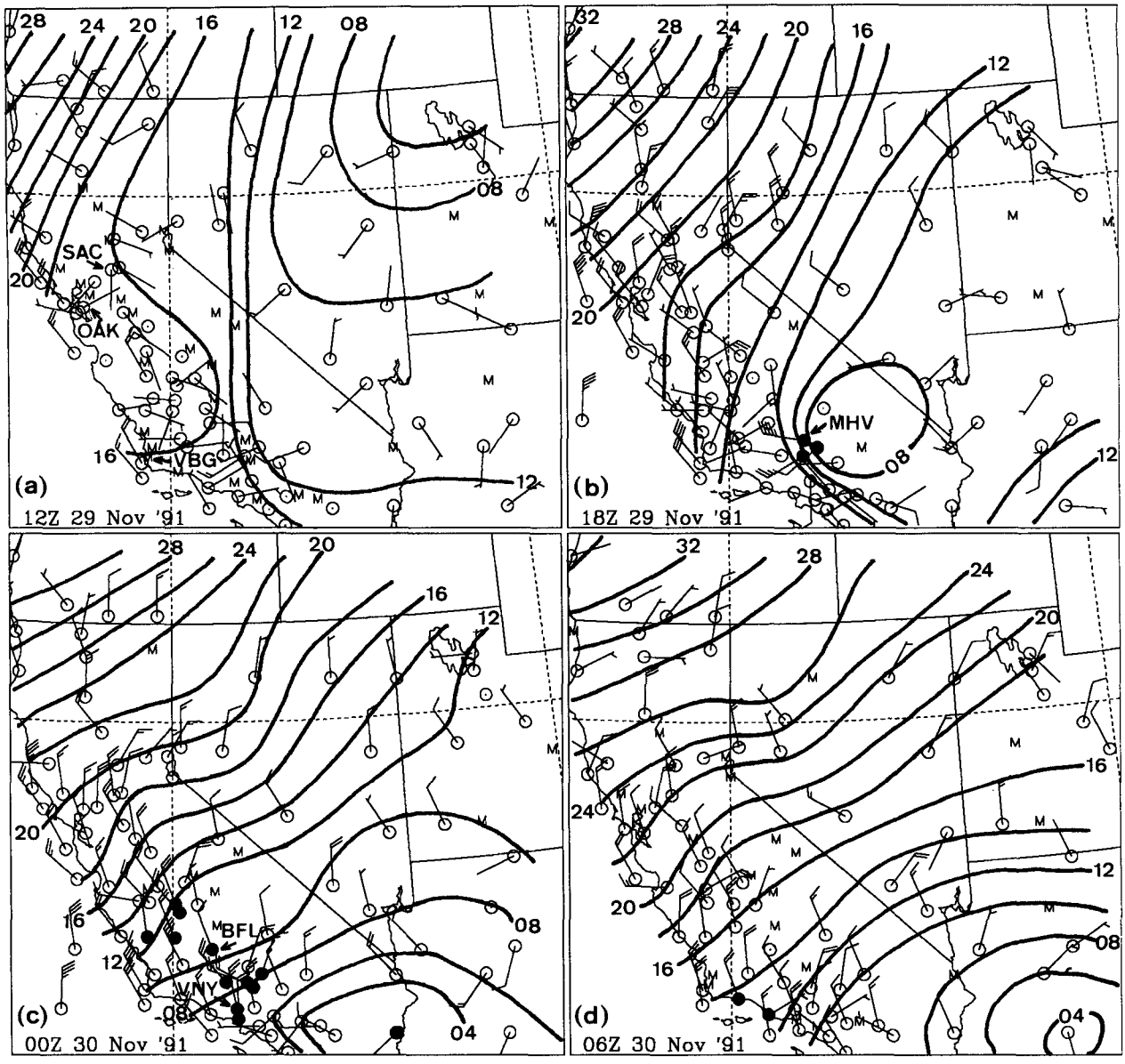

FIG. 10. Manual analyses of sea level pressure from the SA dataset for (a) 1200 UTC 29 November, (b) 1800 UTC 29 November, (c) 0000 UTC 30 November, and (d) 0600 UTC 30 November 1991. Isobars are drawn every 2 hPa and labeled with the last two digits. Winds are plotted from the SA, CIMIS, and RAWS datasets, with a full barb representing 5 m s^{-1} (9.7 kt) and a half barb representing 2.5 m s^{-1} (4.9 kt). Missing observations are indicated with "M," and calm winds with a circle. Solid circles indicate blowing dust reported at an SA station or solar radiation reduced by more than 50 W m^{-2} at a CIMIS station. Some observations were omitted to improve legibility.

0100 UTC; and 0600 UTC 30 November, referred to as the "post-BD" time since BD reports had essentially ended. An analysis of the surface data for 2200 UTC, a half hour before the accidents, is presented in Fig. 11. Surface temperature fields were analyzed but are not shown because of their dependence on terrain height, which varies greatly over the region of interest.

The "predawn" analysis at 1200 UTC (0400 PST) 29 November, approximately 10 h prior to the collisions, portrayed a small-scale ridge extending down the San Joaquin Valley and the coast ranges from the anticyclone offshore and a trough extending into southeastern California from Nevada (Fig. 10a). The ridge had been located along the northern borders of California and Nevada in the 0000 UTC 29 Novem-

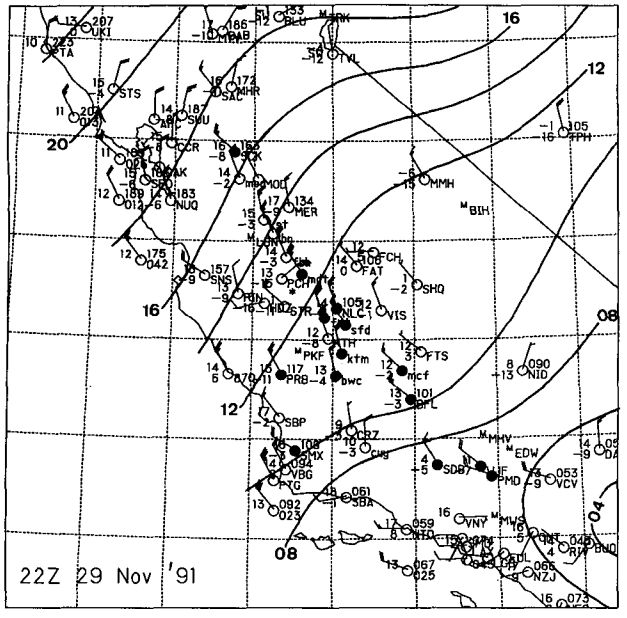

FIG. 11. Manual analysis of sea level pressure for 2200 UTC 29 November 1991. Isobars are drawn every 2 hPa and labeled with the last two digits. Winds are plotted as in Fig. 10. The conventional surface station model is used, with temperature (upper left, °C), dewpoint temperature (lower left, °C), sea level pressure (upper right, 054 implies 1005.4 hPa), and station identifiers (lower right). Solid circles indicate blowing dust reported at an SA station or solar radiation reduced by more than 50 W m^{-2} at a CIMIS station.

ber NCEP analysis (not shown) and propagated southwestward to its current position as it rotated around the eastern flank of the anticyclone. As a consequence of the weak pressure gradient in the ridge, winds were calm or nearly so in central California. The 1200 UTC rawinsonde soundings for Oakland (OAK) and Vandenberg AFB (VBG) depict a steep surface inversion, as would be expected for radiational cooling with light winds (Fig. 12). Surface inversions were also present in the 1300 UTC low-level aircraft soundings for SAC (Fig. 13) as well as for other sites in the San Joaquin Valley (not shown).

By the pre-BD time, 1800 UTC (1000 PST) 29 November, winds in the San Joaquin Valley were picking up and BD reports were starting in the Mojave Desert, with MHV reporting BD, 0.8-km visibility, and winds westerly at 23 m s^{-1} gusting to 31 m s^{-1} at this time. The small-scale ridge previously over the valley had propagated offshore and was replaced by a weak inverted trough (Fig. 10b). In addition, a closed low had formed in the trough in southeastern California with a central pressure of approximately 1005 hPa. The large increase in the pressure gradient in central California was associated both with pressure rises of 2–3 hPa (3 h)$^{-1}$ in northern California and with pressure falls of 2–3 hPa (3 h)$^{-1}$ in the southern California deserts.

By this time, daytime heating had destroyed the early morning surface inversion. The 1900 UTC low-level aircraft sounding for SAC depicted dry adiabatic conditions from the surface to at least 5000 ft (1.5 km) AGL, approximately 840 hPa (Fig. 13). The presence of this adiabatic layer further supports the hypothesized mixing and transport of higher momentum air from the midtroposphere down to the earth's surface. Surface winds in the San Joaquin Valley had indeed increased considerably and had a large cross-isobar component. The surface wind directions were mainly northwesterly, in approximate agreement with the wind direction aloft, as will be discussed in the next section.

By 2200 UTC 29 November, a half hour before the time of the collisions, pressures had fallen across much of the southern half of California, leading to a general northward migration of isobars without much change in the pressure gradient (Fig. 11). The developing low in southeastern California continued to propagate southeastward and is depicted at the edge of Fig. 11 with a central pressure of 1003 hPa. A trough extending westward from the low center had also become apparent in the lee of the San Emigdio, San Gabriel, and San Bernadino Mountains (Fig. 2a). The isobars across the San Joaquin Valley became oriented more southwest–northeast, as the previously mentioned short-wave ridge moved completely offshore. However, the weak inverted trough was still present along the valley except near BFL, where a weak ridge stretched southward. Given this pressure pattern, the strong northwesterly surface winds in the San Joaquin Valley are oriented nearly perpendicular to the isobars, with the strongest winds in the vicinity of the site of the accidents. A comparison of this surface analysis with the satellite image for this time (Fig. 4) shows that the cluster of stations near NLC reporting BD or reduced solar radiation corresponds to the dense plume in the center of the San Joaquin Valley, with a couple of reports farther south in the plume along the western edge of the valley.

At the near-sunset time, 0000 UTC 30 November (1600 PST 29 November), blowing dust reports were ending in the San Joaquin Valley and beginning in the LA Basin. The 0000 UTC soundings for OAK and VBG portrayed adiabatic conditions from the surface to approximately 750 hPa with winds in excess of 30

m s^{-1} at 700 hPa (Fig. 12), while strong northwesterly winds were still present at the surface at many locations in the San Joaquin Valley (Fig. 10c). These observations are consistent with continued boundary layer mixing. The sea level pressure pattern at this time was similar to that at 2200 UTC, with a weak inverted trough over the San Joaquin Valley except near BFL and a low pressure center in southern California. By this time, the low center had propagated to the California–Arizona border near the southern edge of the chart but remained at a central pressure of approximately 1003 hPa. In addition, the trough extending westward from the low center had become sharper with a more pronounced wind shift than at 2200 UTC. The northernmost stations in the LA Basin including previously discussed VNY had strong gusty northerly winds and BD, while the other stations had relatively weak westerlies.

This discontinuity in the wind field separated dry air that was descending the San Gabriel and San Bernadino Mountains from moist onshore flow, although little temperature contrast was present. At 0000 UTC, Santa Monica (SMO), 20 km south of VNY, reported blowing dust, a temperature of 13°C, a dewpoint of −3°C, and winds from 360° at 10 m s^{-1} gusting to 18 m s^{-1}. At the same time, Torrance (TOA), 25 km south of SMO, had a temperature of 15°C, a dewpoint of 8°C, and winds from 300° at 5 m s^{-1}. Although the available data are not sufficient to conclusively determine the cause of this discontinuity, they are consistent with a mountain wave–downslope windstorm event developing in the strong flow crossing the mountains south of the San Joaquin Valley. Wave clouds implying gravity wave activity are present in GOES imagery (not shown) at a number of locations in southern California during this time, including offshore from the LA Basin. Furthermore, the sea level pressure patterns in Figs. 10 and 11 suggest the development of wind-

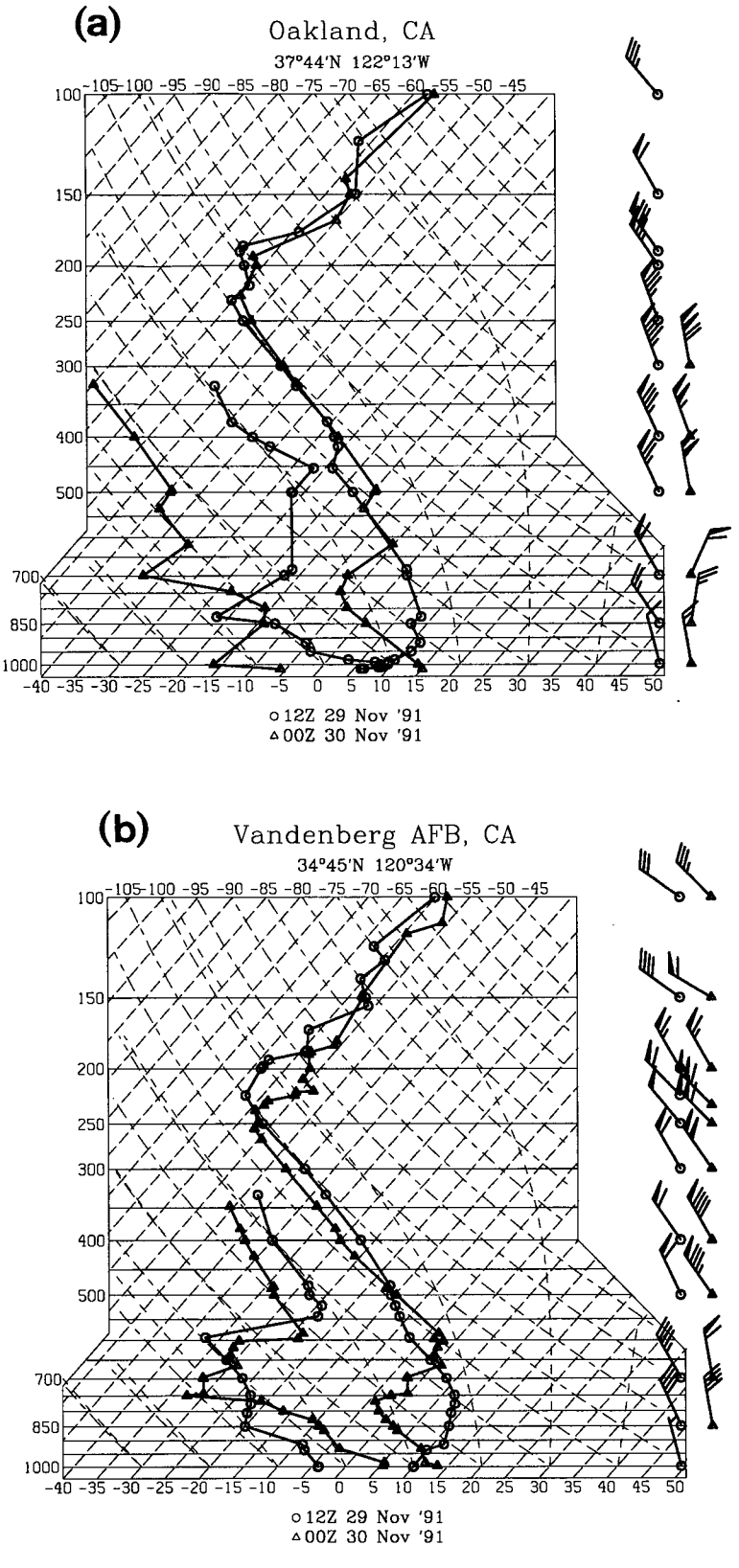

FIG. 12. Soundings plotted on skew *T* diagrams for (a) OAK and (b) VBG. Circles and triangles indicate data from 1200 UTC 29 November and 0000 UTC 30 November 1991, respectively.

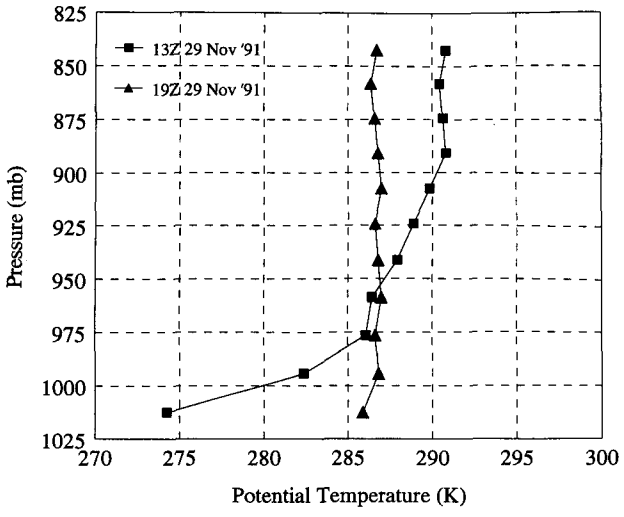

FIG. 13. Potential temperature (°C) from low-level aircraft soundings at SAC. Squares indicate data from 1300 UTC (0500 PST) 29 November 1991; triangles indicate data from 1900 UTC (1100 PST) 29 November 1991.

ward ridging in the southern San Joaquin Valley and lee troughing in the LA Basin in response to the strong flow across the mountains, either through quasigeostrophic processes (Bluestein 1993, 12) or gravity wave processes (Durran 1986). The San Emigdio, Tehachapi, and San Gabriel Mountains that separate the southern San Joaquin Valley from the LA Basin reach heights up to 2600, 2300, and 2900 m, respectively (Fig. 2a). Unfortunately, no soundings are available near 0000 UTC in the San Joaquin Valley to portray conditions upstream of the mountains. However, the 0000 UTC 30 November sounding at nearby VBG on the coast (Fig. 12b) depicts northwesterly winds in a deep layer increasing with height up to 250 hPa and a stable layer based close to mountain-top level (750 hPa) with near-adiabatic conditions above and below, conditions favorable for strong mountain waves (Durran 1986).

By the post-BD time, 0600 UTC 30 November, the developing cyclone had propagated to central Arizona and attained a central pressure of nearly 1002 hPa (Fig. 10d). The trough extending westward from the low center was still present but had shifted southward to a position midway between Los Angeles and San Diego (i.e., the southern edge of the chart) leaving northerly to northwesterly winds in its wake throughout the LA Basin. Although strong northerly winds were still present at some locations, wind speeds decreased overall and the blowing dust reports essentially ended as night fell. No 0600 UTC soundings were available, but the surface cooling and overall decrease in wind speeds implies that a surface inversion has been established and with it a decoupling of the boundary layer from the free atmosphere.

Taken as a whole, these analyses and the observations discussed in the previous section show no evidence of a surface front passing through the San Joaquin Valley. Wind shifts occurred at a number of locations approximately at the onset of the strong winds but in a manner more consistent with heating-induced mixing than a frontal passage. The only indication of a trough in the San Joaquin Valley was the inverted trough oriented along the valley after about 1800 UTC. The lowest pressure at a particular station resulted from the northward advance of the isobars and the development of the inverted trough rather than a front.

5. Upper-level synoptic conditions

The previous discussion presented evidence that daytime boundary layer mixing was present in a deep layer during this case. The companion hypothesis—that upper-level processes associated with a strong jet streak, upper front, and tropopause fold transported momentum downward to a level where it could become involved in mixing—is examined in this section. A jet streak is important in this context, both in terms of providing a momentum source aloft and in terms of the descent associated with its secondary circulations. Furthermore, an upper front is expected to accompany a jet streak according to thermal wind balance, which relates the vertical shear of the geostrophic wind to the horizontal temperature gradient. Frontogenesis aloft generally results from adiabatic warming in descent on the warm side of the front (Keyser and Shapiro 1986) and can reinforce the descent in regions where the isotherms are oriented at an angle to the flow in such a manner as to yield cold advection. Strong descent in the upper troposphere also acts to bring stratospheric air down to lower levels, forming a tropopause fold. Whenever the downward motion associated with these features occurs in a region where the wind speeds increase with height, momentum should be transferred downward.

During the period of interest in this case, the upper troposphere was marked by a strong jet streak, short-wave trough, upper front, and tropopause fold that were propagating southward in meridional flow between an amplifying long-wave ridge over the east-

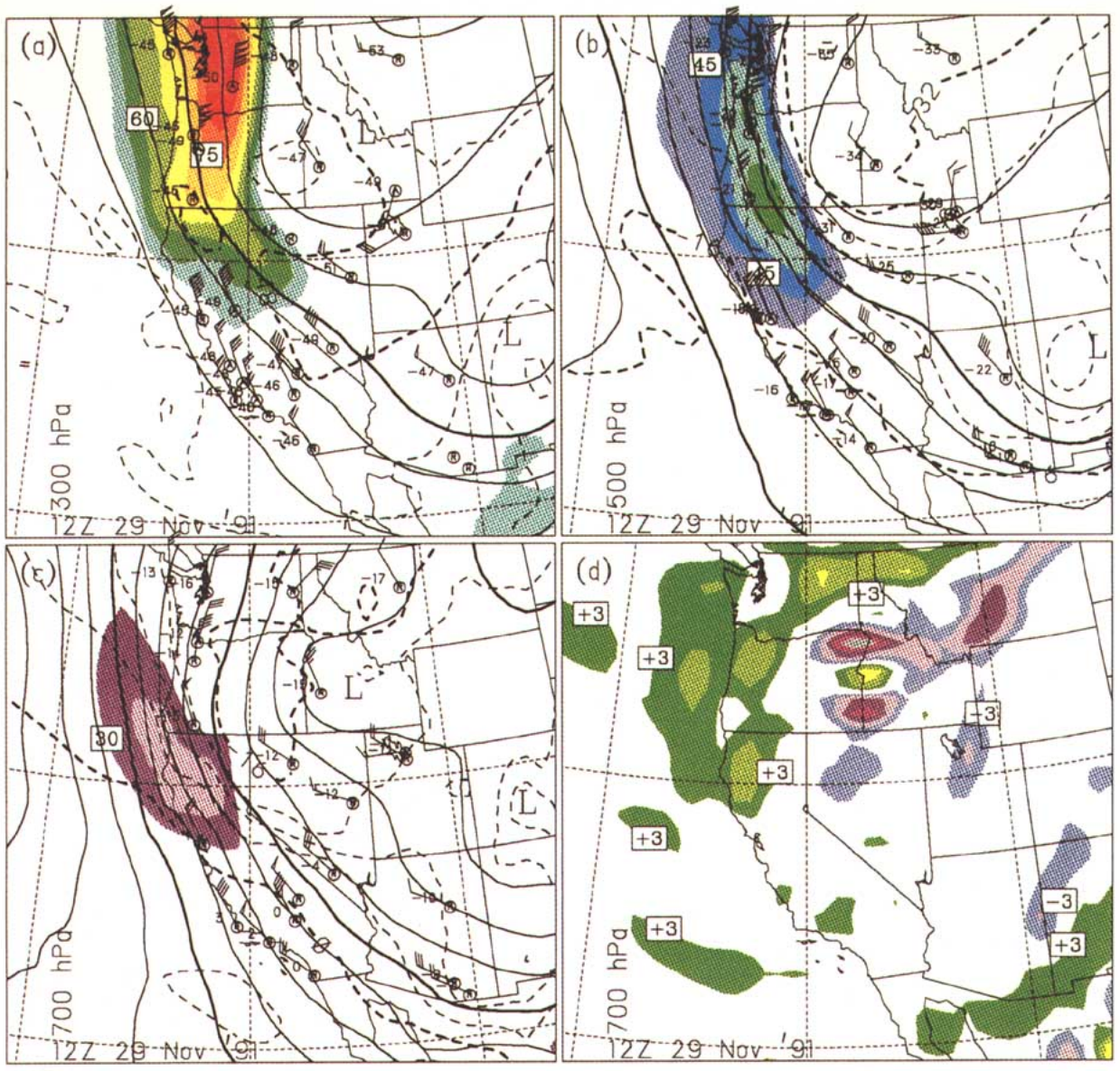

FIG. 14. NORAPS analyses for 1200 UTC 29 November 1991 of heights (solid, m), temperatures (dashed, °C), and wind speed (shaded, m s^{-1}) for (a) 300 hPa, (b) 500 hPa, and (c) 700 hPa, as well as (d) 700-hPa isobaric vertical motion (shaded, μbar s^{-1}). Contours at 300 hPa are drawn with a 120-m interval and with a bold contour at 9120 m, at 500 hPa with a 60-m interval and with bold contours at 5520 and 5760 m, and at 700 hPa with a 30-m interval and with bold contours at 3000 and 3120 m. Isotherms are drawn with a 4°C interval and with bold isotherms at −48°C at 300 hPa, at −32° and −16°C at 500 hPa, and at −16° and 0°C at 700 hPa. Isotachs are shaded with a 5 m s^{-1} interval beginning at 40 m s^{-1} at 300 hPa, at 30 m s^{-1} at 500 hPa, and at 20 m s^{-1} at 700 hPa. The vertical motion field is shaded with a 3 μbar s^{-1} interval beginning at +3 μbar s^{-1} for downward motion and at −3 μbar s^{-1} for upward motion. Winds are plotted with a flag representing 25 m s^{-1} (48.5 kt), a full barb representing 5 m s^{-1} (9.7 kt), and a half barb representing 2.5 m s^{-1} (4.9 kt). Plotted numbers are temperatures (°C) from rawinsonde and ACARS reports. The letter inside the station circle indicates the type of observation, with R for RAOB, A for ACARS, and F for other aircraft observations. ACARS observations within ±3 h of the stated time and within approximately ±25 hPa of the given pressure level are plotted. Some ACARS observations were omitted to improve legibility.

ern Pacific and a long-wave trough over the southwestern United States. Figures 14–17 depict observations and NORAPS analyses of winds, heights, and temperatures at 300, 500, and 700 hPa, along with 700-hPa vertical motions for 1200 UTC 29 November, 1800 UTC 29 November, 0000 UTC 30 November, and 0600 UTC 30 November 1991, respectively, the same times presented in Fig. 10. These vertical motions were produced by the NORAPS mesoscale data assimilation system after initialization and with a

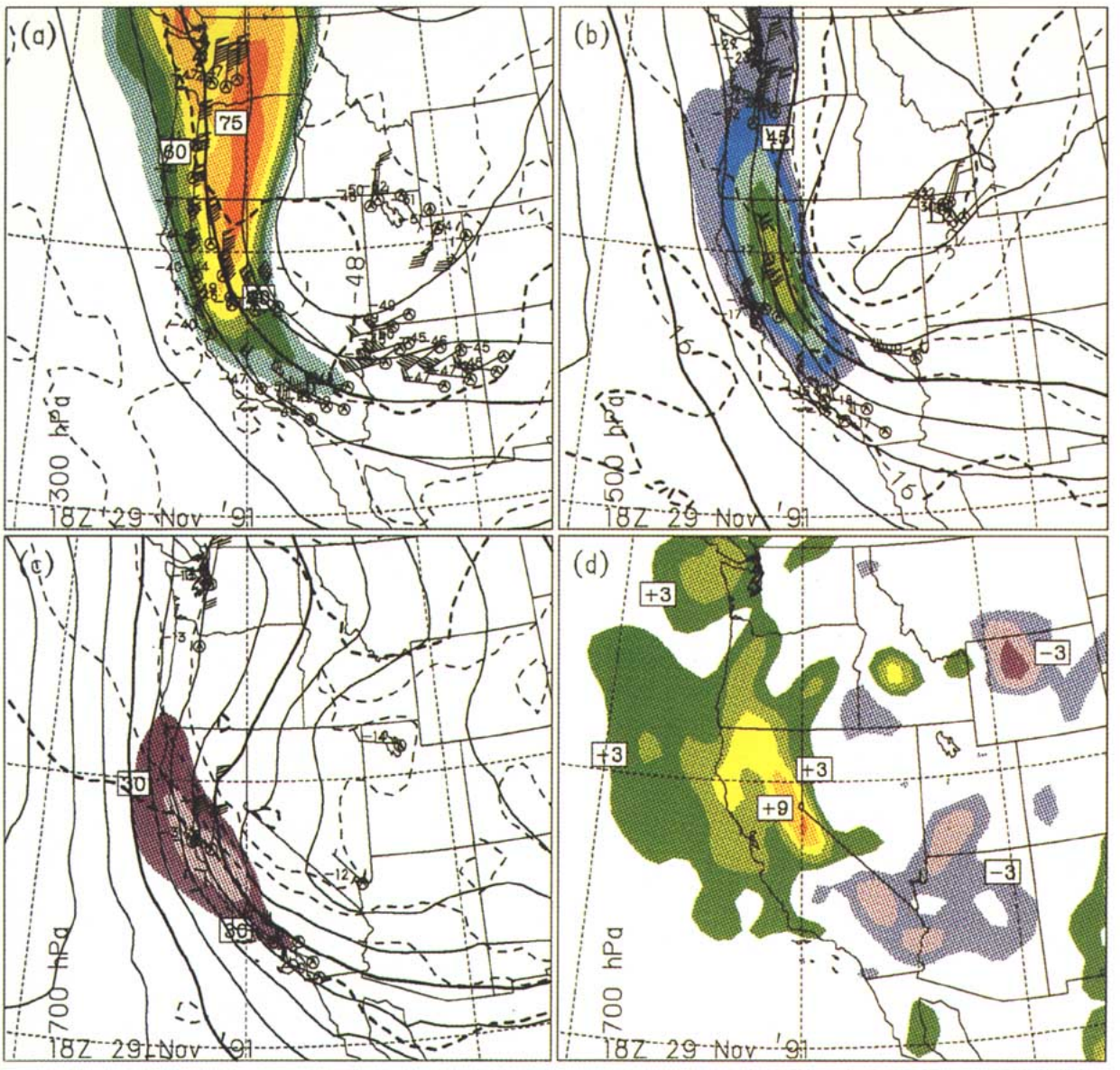

FIG. 15. Same as Fig. 14 except for 1800 UTC 29 November 1991.

single pass of a Shapiro (1977) smoother–desmoother applied to reduce noise without removing mesoscale details.

At 1200 UTC 29 November, the predawn time, the 300-hPa jet streak was centered over Washington state just upstream of the short-wave trough with a maximum speed of 85–90 m s^{-1} (Fig. 14a). The Salem, Oregon, and Medford, Oregon, rawinsonde soundings (RAOBs) just south of the maximum did not report winds at 300 hPa as often occurs in strong jet streaks, but ACARS winds with speeds as high as 85 m s^{-1} were present in central Washington. The wind speed maxima at 500 and 700 hPa were located progressively farther south, with maximum values of 55–60 and 35–40 m s^{-1}, respectively (Figs. 14b,c).

A significant upper front was depicted at 500 hPa as a region of strong temperature gradient extending from northwestern Washington into northern Nevada in the cyclonic shear associated with the jet streak (Fig. 14b). The 700-hPa upper front was located southwest of its 500-hPa position, stretching from western Oregon into southern Nevada (Fig. 14c). The analyses portray the isotherms in the upper front with more of a northwest–southeast orientation than the geopotential contours especially at 700 hPa, implying geostrophic cold advection.

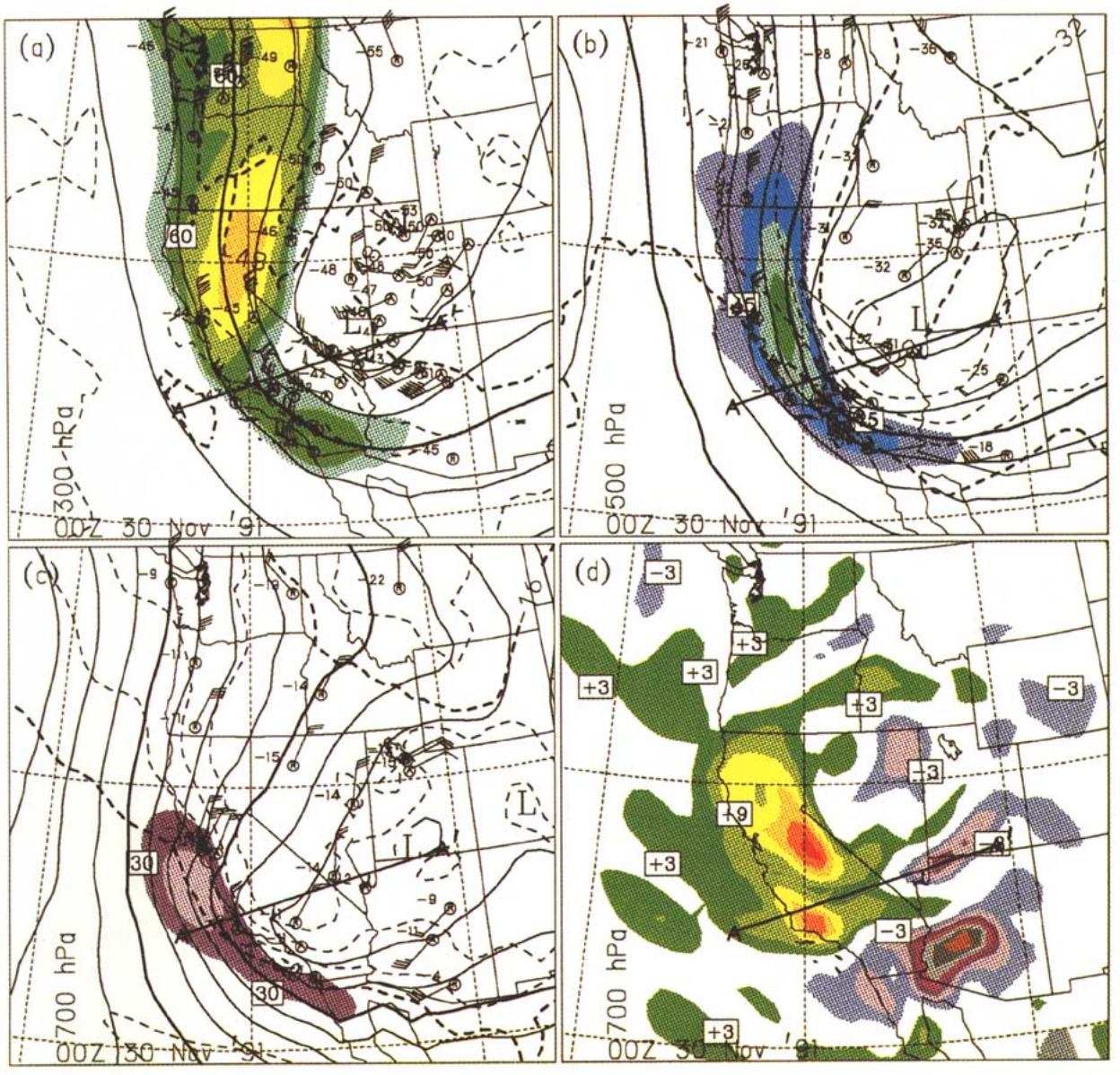

FIG. 16. Same as Fig. 14 except for 0000 UTC 30 November 1991. Line A–A′ indicates the location of the cross section shown in Fig. 21.

At this predawn time, the 700-hPa vertical motion field depicts descent maxima over northeastern Washington, western Oregon, northern California, and just offshore (Fig. 14d). Conventional quasigeostrophic reasoning (e.g., Holton 1979, 138) yields the expectation of anticyclonic vorticity advection (increasing with height) and downward motion in the region between an upper-level ridge and its downstream trough. A comparison of the vertical motion field with the 700-hPa analysis shows that the region of downward motion is indeed located upstream of the short-wave trough except for the maximum over northern California, which is actually downstream of the trough line. On the other hand, in the absence of curvature in the flow, upper-level convergence and tropospheric downward motion are expected in the right-front and left-rear quadrants of a jet streak (e.g., Uccellini 1990). A comparison of the vertical motion field with the 300-hPa wind speeds shows that the northern California maximum is in the right-front quadrant of the jet streak. Ageostrophic winds in the exit region of a jet streak are expected to have a component toward higher geopotential heights, which would contribute to cold avection and descent. Geostrophic cold advection associated with the 700-hPa front also exists in this region and would contribute to descent, as would

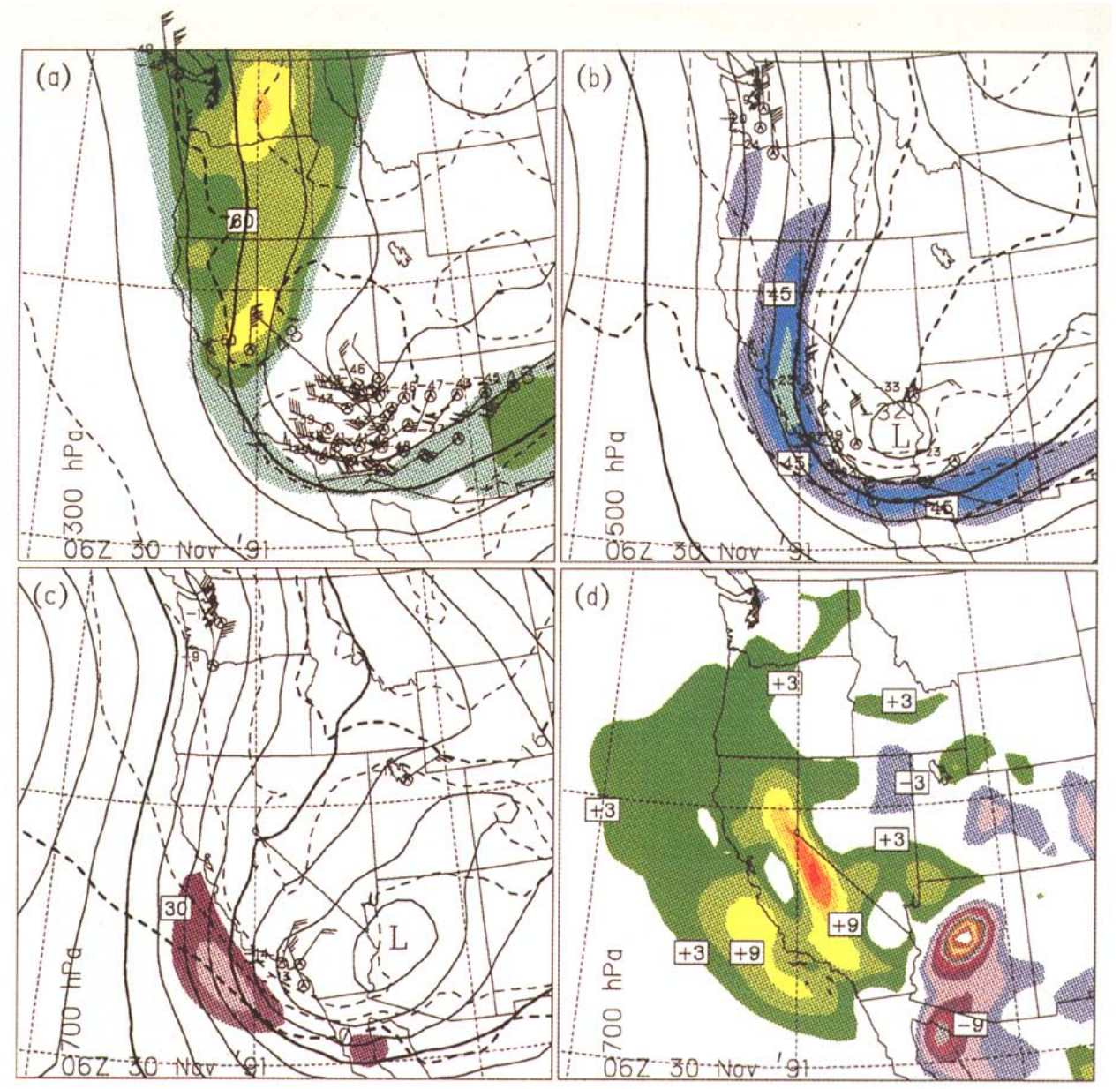

FIG. 17. Same as Fig. 14 except for 0600 UTC 30 November 1991.

downslope flow at the lower boundary. The northern California descent maximum, therefore, is consistent more with jet streak and frontal processes than with quasigeostrophic processes and is in a location coincident with the 700-hPa wind speed maximum, implying downward momentum transport.

By the pre-BD time, 1800 UTC 29 November, the short-wave trough, jet streak, and upper front had propagated southward several hundred kilometers (Fig. 15). Although the analyzed 300-hPa wind speeds had weakened to a maximum of 75–80 m s^{-1}, the 500-hPa wind speeds had strengthened to over 60 m s^{-1}. The 700-hPa winds at this time exceeded 30 m s^{-1} along most of the California coast extending inland over the northern San Joaquin Valley just as the boundary layer mixing and strong surface winds were beginning. The temperature gradient defining the 500-hPa front had strengthened over the previous 6 h as it moved southward, with the largest gradient at this time along the California–Nevada border. At 700 hPa, the upper front extended from the northwestern corner of California to the California–Arizona border.

The downward motion had strengthened to more than 12 μbar s^{-1} over the western slopes of the Sierra

Nevada by this time (Fig. 15d). This maximum is located near the eastern edge of the upper front where some cold advection is present and upstream of the 700-hPa trough where anticyclonic vorticity advection is expected but it also appears to reflect an increase in the downslope component of flow at low levels and hence the terrain-induced vertical motion. A second relative maximum in downward motion exists along the California coast, associated with the right-front quadrant of the jet streak and with cold advection in the upper front. This relative maximum overlaps the 700-hPa wind speed maximum and so likely would have acted to transport momentum downward.

The 300-hPa features continued to propagate southward at 0000 UTC 30 November, the near-sunset time, with the short-wave trough coming in phase with the long-wave trough and yielding highly curved flow (Fig. 16a). The wind speed maximum was located over northern California upstream of the trough; the greatest winds in this location were only 70–75 m s^{-1}, continuing the previously noted weakening trend. However, the high wind speeds extended downstream past the trough line with a secondary maximum in southern California. The maximum 500-hPa winds at this time were also analyzed somewhat weaker than at 1800 UTC (Fig. 16b). The wind speed maximum had moved toward the coast and extended downstream southward and eastward, so that wind speeds decreased over the San Joaquin Valley but strengthened to 50 m s^{-1} along the coast and in Southern California. As a result, the 500-hPa winds over the LA Basin were strongest at this time, just as blowing dust reports were beginning in that location. During this same period, the 700-hPa wind speed maximum had also shifted offshore from the central California coast and extended downstream (Fig. 16c).

The upper front continued to propagate southward, so that the strongest temperature gradient at 500 hPa was located over the San Joaquin Valley and the strongest gradient at 700 hPa extended down the Coast Ranges and along the south coast at this near-sunset time (Figs. 16b,c). The 700-hPa front therefore moved southward through the San Joaquin Valley during the time that blowing dust, high surface winds, and surface dewpoint decreases were present. The northwestern half of the upper front was characterized by cold advection as before, but the southeastern half had neutral or slight warm advection downstream of the trough.

The 700-hPa vertical motion field at the near-sunset time portrayed downward motion over most of California with two maxima—one over the western slopes of the Sierra and one centered just east of VBG (Fig. 16d). While the maximum associated with the Sierra is farther south and stronger than it was at 1800 UTC, it still appears to result in large part from terrain-induced descent at the lower boundary perhaps aided by anticyclonic vorticity advection. The southern maximum is in a region of strong cold advection associated with the upper front and may also have a contribution by downslope flow at the lower boundary. However, this maximum is essentially below the 300-hPa jet axis rather than the right-front quadrant as before. Although the descent maxima are well east of the 700-hPa wind speed maximum, significant downward motion is collocated with the wind speed maximum. A prominent upward motion maximum is also present over southern Arizona, in the vicinity of the developing low center. Ascent in this region is associated with cyclonic vorticity advection and weak warm advection. The resulting adiabatic cooling on the warm side of the front is frontolytical, as reflected by the slackening of the 700-hPa temperature gradient in southeastern Arizona at this time.

The post-BD time, 0600 UTC 30 November, portrays a further weakening of the 300-hPa winds, yielding speeds over California less than 70 m s^{-1}, and the expansion of a second maximum downstream of the trough over New Mexico (Fig. 17a). The weakening and appearance of a downstream maximum was also seen at 500 hPa, with a 50–55 m s^{-1} maximum upstream of the trough line and a 45–50 m s^{-1} maximum downstream (Fig. 17b), and at 700 hPa as well, with twin maxima south of the 500-hPa maxima (Fig. 17c). The jet streak appears to be trying to propagate past the long-wave trough line, but wind speeds weaken even though the height gradient and therefore the geostrophic wind remain strong. Gradient wind balance in this case would require a decrease in wind speed as the curvature of the flow increases, and so the jet streak appears to be dissipating upstream of the trough and forming again downstream of the trough. The short-wave trough, geostrophic wind speed maximum (not shown), and upper front, however, are able to maintain continuity as they propagate through the long-wave trough.

The strongest 500-hPa temperature gradient was passing the trough line in southern California in a region of significant cyclonic curvature, with the 700-hPa gradient displaced to its southwest (Figs. 17b,c). An aircraft with ACARS capability flying near the

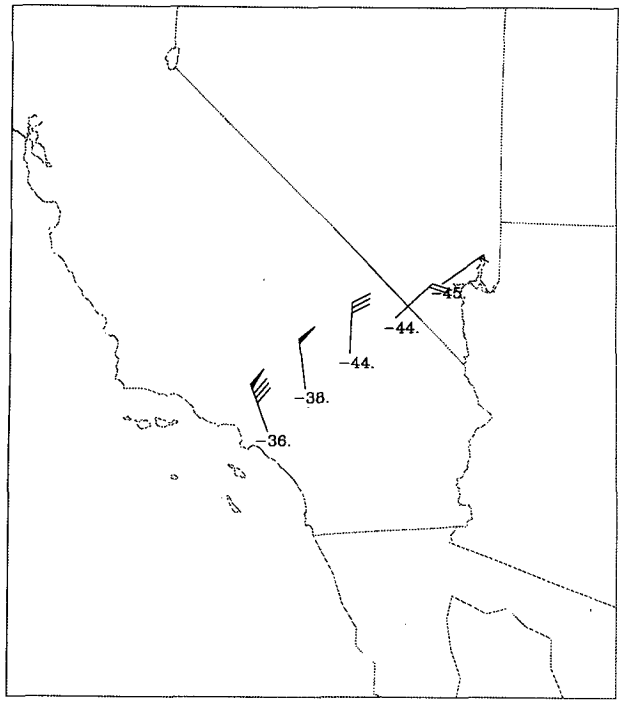

FIG. 18. ACARS observations from Northwest N515 as it traversed the upper front in southern California. Winds are plotted following the convention described in Fig. 14, while plotted numbers are temperatures in °C. The aircraft was traveling in a northeastward direction at pressure altitudes of 7650 to 7620 m (approximately 400 hPa) between 0728 and 0758 UTC 30 November 1991. Observations are spaced 7.5 min apart, a distance of approximately 90 km. Note the strong cyclonic shear and large temperature gradient.

400-hPa level crossed the upper front in southern California between 0728 and 0758 UTC (Fig. 18). These observations, spaced approximately 90 km apart, depict strong cyclonic shear, with speeds decreasing successively from 40 to 25 to 15 m s^{-1}, and an intense upper front, with temperatures decreasing successively from −36° to −38° to −44°C.

The 700-hPa vertical motion field was similar to that at 0000 UTC, with a strong descent maximum over the western slopes of the Sierra, a second descent maximum just offshore from central and southern California, and a strong ascent maximum in central Arizona (Fig. 17d). The descent in the lee of the Sierra appears to be associated with terrain effects, while the descent offshore appears to result from the right-front quadrant of the jet streak and from the strong cold advection in the upper front. As before, the latter maximum overlaps with the 700-hPa wind speed maximum, suggesting continued downward transport of momentum.

The relationship between the upper front and its associated tropopause fold can be seen by comparing Figs. 14 and 16 with Fig. 19, which depicts the tropopause pressure reported by RAOBs and the pressure at the 3.0×10^{-6} K m^2 kg^{-1} s^{-1} (referred to as 3.0 PVU) potential vorticity surface computed from the NORAPS analysis. Spaete et al. (1994) compared reported tropopause pressures to pressures computed for potential vorticity surfaces in the 1.6–4.0-PVU range using model output and found that defining the tropopause as the 3.0-PVU surface yielded the minimum root-mean-square differences, even though a value of 1.6 PVU is more commonly used (e.g., WMO 1986). The tropopause pressure was computed for the current case as the lowest pressure (i.e., the pressure corresponding to the highest altitude) at which 3.0 PVU was found, a method similar to that used by Spaete et al. (1994). If the potential vorticity was less than 3.0 PVU at all levels below 100 hPa, the pressure was set to 100 hPa. This method for defining tropopause pressure does not permit multiple values as would occur at a tropopause fold but does hint at the existence of a fold by portraying a large pressure gradient and so a nearly vertical orientation to the tropopause (e.g., Spaete et al. 1994, Fig. 1).

The overall pattern of analyzed tropopause pressures at the 1200 UTC 29 November predawn time shows a prominent maximum greater than 450 hPa associated with the upper-level trough, in contrast to values generally less than 200-hPa offshore (Fig. 19a). The gradient was concentrated in central Washington and Oregon, with a change of 100 hPa essentially between neighboring grid points collocated with the strong cyclonic shear just west of the 300-hPa temperature maximum (Fig. 14a). The temperature maximum is indicative of the stratospheric air expected where the analyzed tropopause drops below the 300-hPa surface. The large gradient is also located approximately over the 500-hPa front, as would be expected for a tropopause fold.

The tropopause analysis for the near-sunset time (0000 UTC 30 November) depicts a maximum of 500 hPa, considerably greater (i.e., closer to the surface) than earlier (Fig. 19b). The maximum maintained its identity with the trough and the 300-hPa temperature maximum, the latter of which was warmer than earlier (Fig. 20a). A warmer 300-hPa temperature maximum is consistent with the deeper layer of increasing temperatures in the stratosphere above a lower tropopause. The reported tropopause was as low as 400 hPa at Mercury, Nevada, west of the maximum (Fig. 20b).

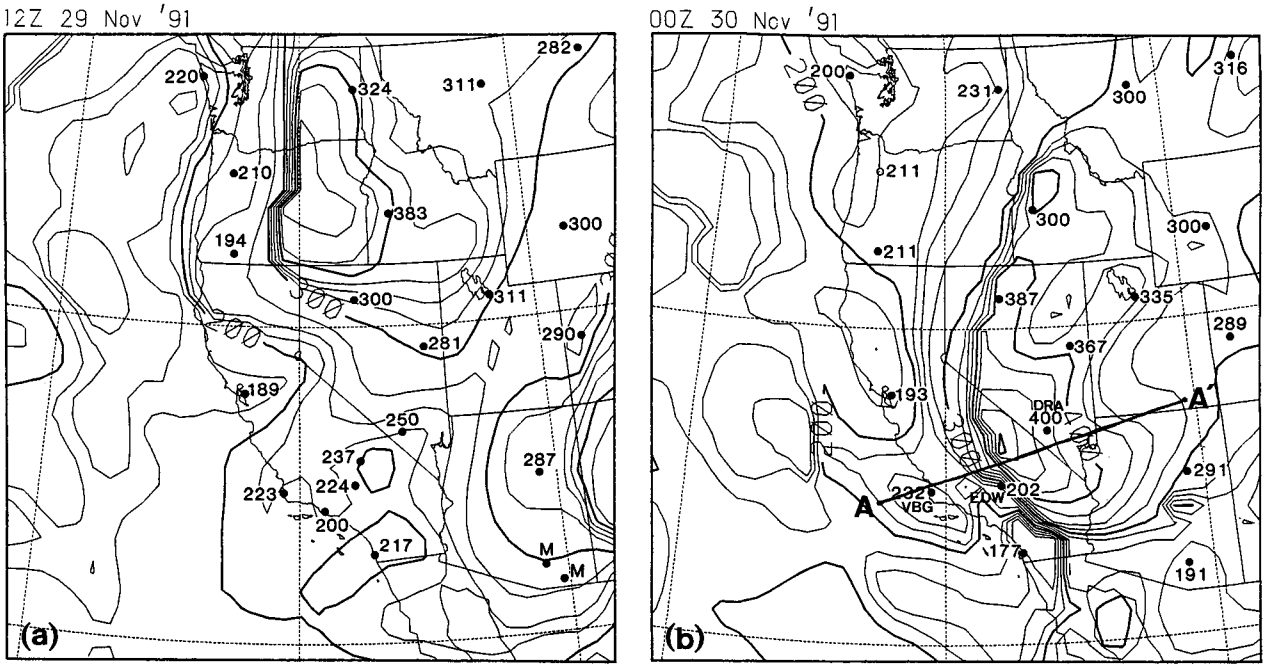

FIG. 19. NORAPS analyses of tropopause pressure (hPa) for (a) 1200 UTC 29 November and (b) 0000 UTC 30 November 1991. The analyzed tropopause is defined as the 3.0-PVU surface. Plotted values are tropopause pressures (hPa) reported in rawinsonde observations. Line A–A′ indicates the location of the cross section shown in Fig. 21. The three soundings plotted on the cross section are also indicated by their station identifiers—VBG for Vandenberg AFB; EDW for Edwards AFB; and DRA for Mercury.

The strong gradient of tropopause pressure southwest of the maximum agrees best with the 300-hPa cyclonic shear and the 500-hPa front, and so most likely represents the tropopause fold. The stronger gradient farther south is exaggerated by the artificial values of 100 hPa near the Mexican border.

A cross section through the tropopause pressure maximum and within 100 km of the soundings at Vandenberg, Edwards, and Mercury is shown in Fig. 21. The sloping upper front is apparent in this cross section as the stable layer centered approximately at the 300-K isentrope west of Mercury. An examination of the horizontal analyses (Fig. 16) shows that Vandenberg was near the center of the 700-hPa front at this time, while Edwards was near the center of the 500-hPa front. The upper front appears as a dry stable layer in the 0000 UTC Vandenberg (Fig. 12b) and Edwards soundings (Fig. 20a) at 750–600 and 600–500 hPa, respectively. The stratospheric air in the tropopause fold, depicted by the 3.0-PVU isopleth in the cross section, was coincident with the upper front and located on the cyclonic shear side of the jet streak, as previously noted. In addition, the cross section portrays weak stability below the upper front, where potential temperature varied only slightly from 288 K. The soundings for Vandenberg, Edwards, and Mercury in Figs. 12 and 20 depict essentially adiabatic conditions from the surface to at least 750 hPa.

The 1.6-PVU isopleth is shown for comparison as an alternate definition of the tropopause; it also follows the upper front on the cyclonic shear side of the jet streak, extending as low as 750 hPa at Vandenberg. If the 1.6-PVU surface portrays the actual tropopause, then the base of the inversion in the Vandenberg sounding at approximately 750 hPa would correspond to the tropopause. The tropopause reported at 232 hPa then reflects the uppermost occurrence of the tropopause. The upper inversion is reported as the tropopause rather than the lower inversion because of the 2-km-depth requirement imposed in the WMO (1988) definition.

In summary, the upper-level data and analyses for this case portray a jet streak, short-wave trough, upper front, and tropopause fold propagating southward, approaching and then passing the long-wave trough during the period examined. As required by gradient wind constraints, the wind speeds associated with the jet streak decreased dramatically as the features passed the long-wave trough even though the height gradient in the trough remained strong. The wind speed

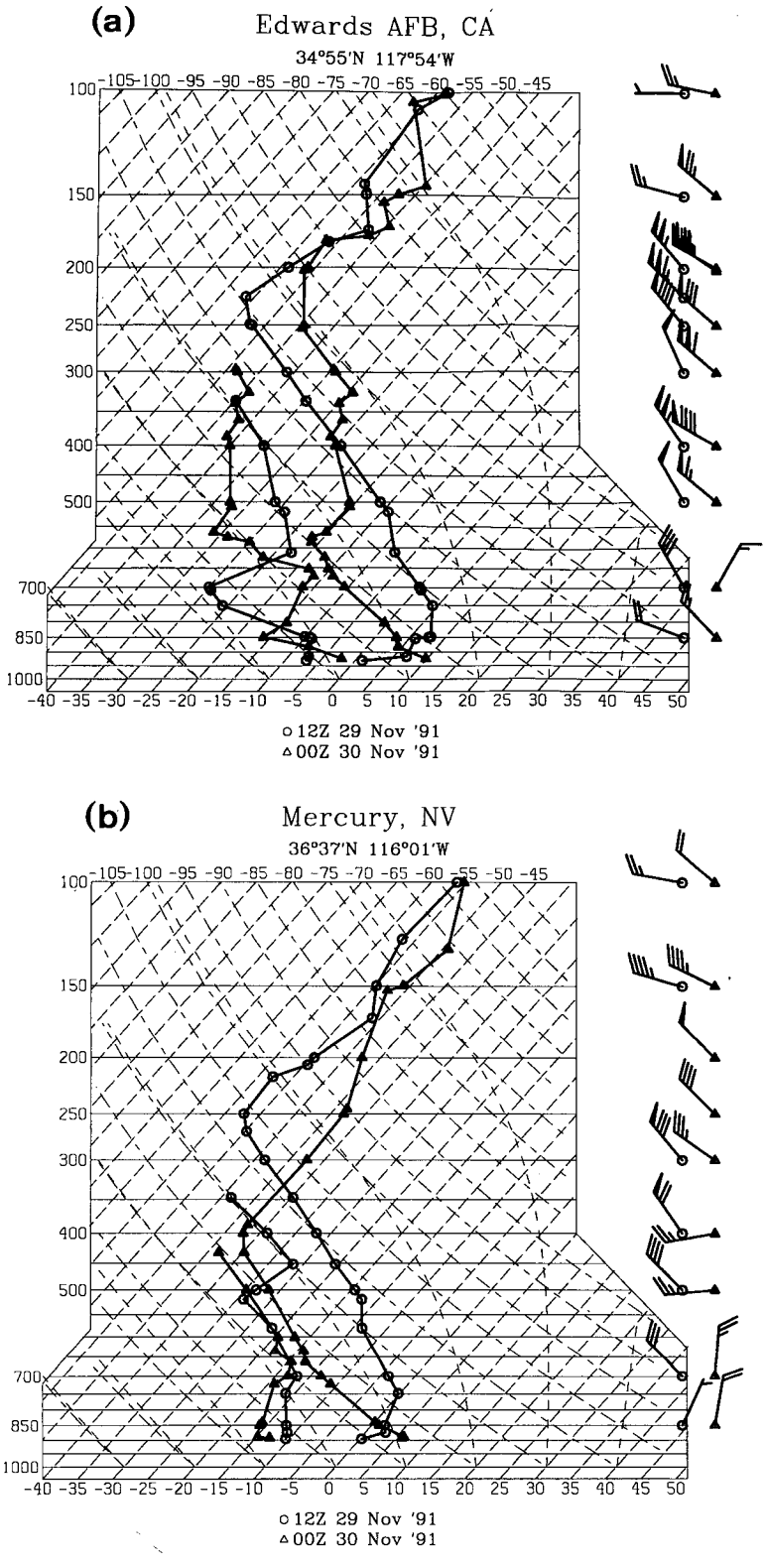

FIG. 20. Same as Fig. 11 except for (a) Edwards AFB and (b) Mercury.

maximum therefore weakens upstream of the trough and strengthens again downstream of the trough. Even so, the upper front and tropopause fold increased in strength during the same period, consistent with sustained strong downward motion aloft. The downward motion on the warm side of the upper front appeared to result primarily from jet streak processes and cold advection. The close association of this descent maximum and the 700-hPa wind speed maximum supports the hypothesized role of downward momentum transport.

6. Discussion and summary

This case study focused on the meteorological conditions of 29 November 1991 that led to near-zero visibility in blowing dust and a series of multiple-vehicle collisions on I-5 in the San Joaquin Valley. The drought conditions that had prevailed in that area for six years and the late onset of the rainy season in 1991 made blowing dust an all but inevitable consequence of the high winds that were present that day. This paper examined the observations for this case and presented evidence for the hypothesis that intense upper-tropospheric downward motion led to the formation of a strong upper front and tropopause fold and transported high momentum air downward to midlevels where boundary layer processes could then mix it to the surface.

These high surface winds were forecast; the National Weather Service had issued a wind and blowing dust advisory for the west side of the southern San Joaquin Valley as early as 0830 PST, as well as a high wind warning for the Mojave Desert as early as 0925 PST. These messages were updated throughout the day as the event unfolded. Nevertheless, a number of actions were implemented following the investigation of the accidents, including changeable message signs to better advise motorists of conditions, a more consistent policy for California Highway Patrol escorts to pace traffic during low-visibility conditions, cover crops on fallow land adjacent to the highway to reduce dust

generation, and automated weather stations with visibility detection along the interstate (State of California 1992).

This paper documents the blowing dust event using SA and RAOB data, ACARS winds, and other surface observations and low-level soundings. The results show that blowing dust was observed or inferred at numerous locations in the San Joaquin Valley, in the Mojave and other desert locations, and along the south coast, including the LA Basin. The blowing dust and high winds began at the valley and desert sites nearly simultaneously before local noon and ended near local sunset, supporting a role for boundary layer mixing induced by surface heating. RAOB soundings taken at 0000 UTC 30 November confirmed an adiabatic lapse rate below 750 hPa at OAK and VBG and below 575 hPa at EDW. Furthermore, a low-level sounding at SAC showed that the adiabatic layer was established to 5000 ft AGL by 1900 UTC.

Large decreases in dewpoint temperature were also seen at many sites in the San Joaquin Valley, as would occur by mixing in upper-level air. No sign of a surface front was found in the temperature observations in the valley, but an analysis of dewpoint temperatures showed that the strong drying appeared to propagate through the Central Valley, occurring earliest at the northern end of the valley. This is consistent with the propagation of a dry feature aloft, such as described by Fuelberg et al. (1991), perhaps associated with the upper front that propagates through the San Joaquin Valley during this time.

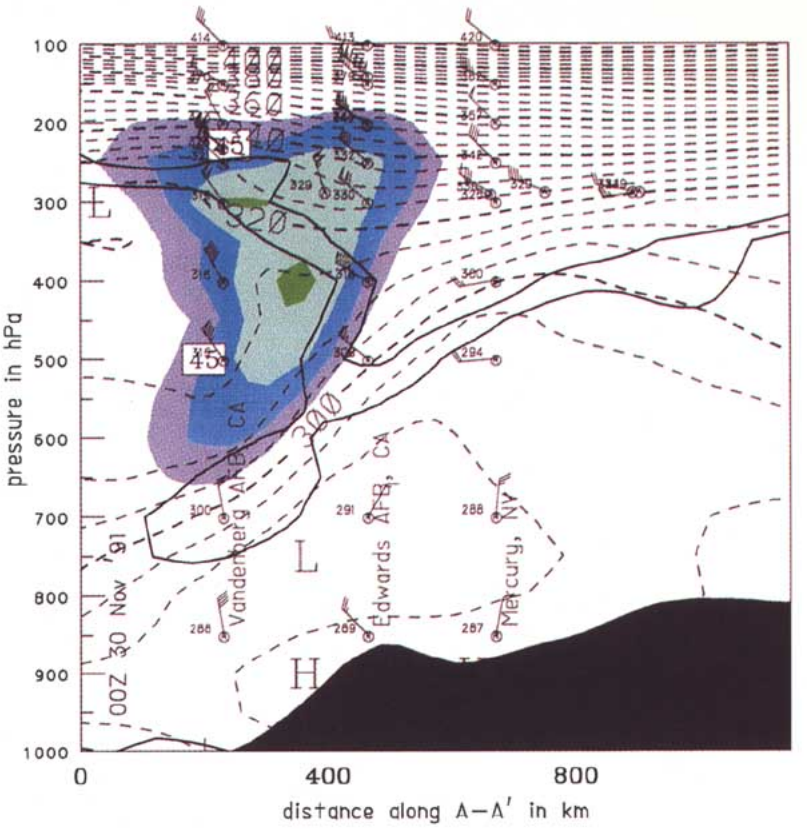

FIG. 21. Cross section of potential temperature (dashed, K), wind speed (shaded, m s^{-1}), and potential vorticity (solid, PVU) from the 0000 UTC 30 November 1991 NORAPS analysis. Isentropes are drawn every 5°C, while isotachs are drawn every 5 m s^{-1} beginning with 40 m s^{-1}. Solid lines represent potential vorticity values of 1.6 (lower) and 3.0 PVU (upper). The plane of the cross section is shown in Figs. 16 and 19b, where the left (right) side of the cross section corresponds to the southwest (northeast) end of line A–A′. Winds are plotted following the convention described in Fig. 14. Potential temperatures for the Vandenberg AFB, Edwards AFB, and Mercury soundings and the ACARS observations are also plotted. ACARS observations within ±3 h of the stated time and within ±120 km of the cross-section plane are plotted.

It is interesting to note that Parkinson (1936) recognized the importance of boundary layer mixing in a study of dust storms over the Great Plains during the Dust Bowl era. The importance of low-level instability and wind speeds greater than 30 mph (13 m s^{-1}) were assumed. Out of his sample of perhaps 50 storms, more than 10 were confined to daylight hours, presumably a result of surface heating leading to boundary layer mixing. He also found a diurnal temperature range of 20°–30°F (11°–17°C) in many cases, similar to the range in this case.

On the other hand, the blowing dust reports along the south coast and in the LA Basin began near sunset in the wake of a mesoscale trough that propagated southward through the evening hours. The sea level pressure pattern portrayed a mesoscale high pressure anomaly in the southern San Joaquin Valley in addition to the trough in the LA Basin, suggesting windward ridging and lee troughing on either side of the rather complex mountains that separate the two. The 0000 UTC 30 November sounding for VBG, the best estimate available for conditions upstream of the mountains, portrayed a stable layer based at 750 hPa

capping an adiabatic layer with a second nearly adiabatic layer aloft. Durran (1986) describes such conditions as favorable for mountain wave development. Although the data do not conclusively verify the presence of mountain waves, GOES imagery did show wave clouds in the vicinity of southern California.

The high surface winds occurred in the context of a strong jet streak and short-wave trough embedded in the northwesterly flow between a high-amplitude ridge over the eastern Pacific and a long-wave trough over the southwestern United States. During the period examined, the jet streak propagated southward, weakened substantially upstream of the trough, and appeared to redevelop downstream of the trough. A strong upper front and tropopause fold were also associated with the jet streak. The upper front was characterized by cold advection initially, with warm advection developing in the southeastern portion of the front as the features approached and passed the upper-level trough.

The combination of cold advection, anticyclonic vorticity advection, and the jet streak exit region's transverse circulation were associated with very strong downward motion, in agreement with Keyser and Shapiro (1986) and Uccellini (1990). Two descent maxima were present—one located over the Sierra that was consistent with terrain-induced descent and quasigeostrophic forcing, the other consistent with the descending branch of the transverse circulation in the exit region of the jet streak and with cold advection from the upper front. The latter maximum was greater on the warm side of the upper front and so acted to strengthen and maintain the upper front. The stratospheric values of potential vorticity present in the tropopause fold were also consistent with strong descent. Analyses of the dynamic tropopause (3-PVU surface) depicted a pressure maximum that increased to more than 500 hPa by 0000 UTC 30 November. In addition, the placement of the 700-hPa wind speed maximum coincided with downward motion, supporting the hypothesized role of downward momentum transport. One noteworthy aspect of this case was that these upper-level processes were acting over the San Joaquin Valley during daylight hours, allowing the interaction with heating-induced mixing.

Topographic effects likely also played a role in this case, although the widespread nature of the strong surface winds suggests a secondary role. The highest surface winds were seen at RAWS stations in the coast range, which tend to be at higher elevations and in more complex terrain than CIMIS or SA stations. The Panoche Road RAWS station immediately west of the accident site had northeasterly winds, in contrast to the northwesterly winds at nearly all of the valley stations. The northeasterly flow was oriented up a side valley and may have made conditions worse by blowing the dust directly across I-5, but it suggests that the flow at the accident site was not accelerated by being channeled through a gap or canyon. The latter yields its highest winds where the flow exits the gap. As discussed earlier, the complex terrain north of the LA Basin likely generated mountain waves, which may have played a key role in producing high surface winds there. In addition, the descent maximum in the lee of the Sierra suggests a significant contribution to the vertical motion by terrain effects.

If the hypothesis proposed to explain the strong surface winds in this case is valid, then other examples should be available both in California and other locations. An examination of the literature on dust storms shows this to be the case. Danielsen (1974) describes a scenario in which a jet streak with wind speeds in excess of 50 m s^{-1} is associated with cold advection and an amplifying upper-level trough. Isentropic trajectories portray air parcels in the jet decelerating and descending to the top of a deep adiabatic layer, where relatively high wind speeds can be mixed to the surface and generate airborne dust. His primary example from April 1963 (Danielsen 1964), however, differs somewhat from the case presented in this paper in that the dust storm occurred ahead of a surface cold front that was coupled with an upper front. In the present case, the blowing dust occurs more or less beneath the jet axis and upper front, with no apparent surface extension of the temperature gradient associated with the upper front.

A case with more similarities to the present case was described by Holets (1990). Strong surface winds occurred in northern California on 14–15 December 1988 leading to numerous power outages, downed trees, and the loss of a 500-ft radio transmission tower. The strong surface winds at 0000 UTC 15 December were northerly and oriented approximately normal to the sea level isobars. The 500-hPa winds at Medford, Oregon, at this time were also northerly and quite strong at nearly 50 m s^{-1}. Blowing dust was also observed in California's Central Valley on 15 October 1994 when a strong upper-tropospheric jet propagated over the state in northerly flow.

The scenario hypothesized to explain the strong surface winds for this case is also similar to that described in Kapela et al. (1995) in their study of strong

wintertime post–cold front winds in the northern plains. Although they do not explicitly discuss the role of the upper front and mesoscale aspects of upper-level descent, their checklist includes among other things the following conditions favorable for a strong wind episode—a strong southeastward-traveling vorticity center, implying a short-wave trough and quasi-geostrophic descent to its rear; destabilization producing near-adiabatic lapse rates in the lower atmosphere; and an approaching upper-level jet streak with little directional shear in the vertical.

A more complete diagnosis of the jet streak and upper-front system in this and related cases is planned for future research, as is an evaluation of the performance of the NORAPS mesoscale data assimilation system. The planned diagnosis will examine the development of the jet streak, upper front, and tropopause fold, including the associated vertical circulation, over a several-day period. A kinetic energy analysis is also proposed in order to more explicitly examine the hypothesized role of downward momentum transport. The roles of boundary layer mixing and topography will be addressed with modeling work using greater horizontal resolution and a second-order closure boundary layer parameterization. Finally, the possibility of a mountain wave generating high surface wind speeds in the LA Basin will be examined using the navy's Coupled Ocean–Atmosphere Mesoscale Prediction System (COAMPS), a nonhydrostatic model with variable resolution as fine as a few kilometers.

Acknowledgments. The authors thank Mr. Bob Godfrey, NRL-Monterey, for retrieving the archived observations and fields for the data assimilation runs; Dr. Geoff DiMego, NCEP, for providing the ACARS data; Dr. Steven Chiswell, North Carolina State University, for providing the coded SAs; Mr. David Moellenberndt, California Department of Water Resources, for providing the CIMIS data; Mr. Jon Butts, California Department of Forestry and Fire Protection, and Mr. Jim Ashby, Western Regional Climate Center, for providing the RAWS data; Mr. Neil Wheeler, Mr. Steve Gouze, and Mrs. Dolores Marchetti, California Air Resources Board, for providing the low-level aircraft soundings; Mr. Jeff Hawkins and Mr. Kim Richardson, for obtaining and processing the AVHRR imagery; Mr. Steve Saville, California Department of Transportation, for providing a copy of the task force report on the accidents; Mr. Steve Bishop, for his assistance in drafting; Prof. Steve Ackerman, for providing the GOES imagery; Mr. Dominique Thongs, Water Resources Program, Princeton University, for providing the high-resolution terrain dataset; and AG[2] David Fishbaugh, NPMOD Lemoore, for providing the precipitation data for Lemoore NAS. The authors also appreciate the discussions with and suggestions by Mr. Dan Gudgel, Warning Coordination Meteorologist for the San Joaquin Valley NEXRAD National Weather Service Office; Dr. Mel Shapiro, NOAA/ETL; Prof. Robert Renard and Mr. Mark Boothe, Naval Postgraduate School; Dr. Teddy Holt, NRL-Monterey; and Mr. Jan Null of the San Francisco National Weather Service Forecast Office; as well as the insightful comments and suggestions concerning the manuscript by Prof. Fred Sanders, Prof. Dan Keyser, and anonymous reviewers. The support of the Office of Naval Research Program Elements 0601153N and 0602435N is gratefully acknowledged.

References

Baker, N. L., 1992: Quality control for the Navy operational atmospheric database. *Wea. Forecasting,* **7,** 250–261.

Barker, E. H., 1992: Design of the navy's multivariate optimum interpolation analysis system. *Wea. Forecasting,* **7,** 220–231.

Benjamin, S. G., K. A. Brewster, R. Brümmer, B. F. Jewett, T. W. Schlatter, T. L. Smith, and P. A. Stamus, 1991: An isentropic three-hourly data assimilation system using ACARS aircraft observations. *Mon. Wea. Rev.,* **119,** 888–906.

Bluestein, H. B., 1993: *Synoptic–Dynamic Meteorology in Midlatitudes.* Oxford University Press, 594 pp.

Danielsen, E. F., 1964: Project Springfield Report. DASA Rep. 1517, Defense Atomic Support Agency, Washington, DC, 97 pp.

——, 1974: The relationship between severe weather, major dust storms, and rapid large-scale cyclogenesis. *Subsynoptic Extratropical Weather Systems: Observations, Analysis, Modeling, and Prediction,* Vol. 2, M. Shapiro, Ed., National Center for Atmospheric Research, 215–225.

——, 1975: The generation and triggering of severe convective storms by large-scale motions. *Open SESAME, Severe Environmental Storms and Mesoscale Experiment, Proc. of the Opening Meeting,* Boulder, CO, NOAA/ERL, 165–185.

Durran, D. R., 1986: Mountain waves. *Mesoscale Meteorology and Forecasting,* P. S. Ray, Ed., Amer. Meteor. Soc., 472–492.

Fuelberg, H. E., R. L. Schudalla, and A. R. Guillory, 1991: Analysis of sudden mesoscale drying at the surface. *Mon. Wea. Rev.,* **119,** 1391–1406.

Gillette, D. A., J. Adams, A. Endo, and D. Smith, 1980: Threshold velocities for input of soil particles into the air by desert soils. *J. Geophys. Res.,* **85**(C10), 5621–5630.

Hall, F. F., 1981: Visibility reductions from soil dust in the western U.S. *Atmos. Environ.,* **15,** 1929–1933.

Hess, S. L., 1959: *Introduction to Theoretical Meteorology.* Holt, Rinehart and Winston, 362 pp.

Hodur, R. M., 1987: Evaluation of a regional model with an update cycle. *Mon. Wea. Rev.,* **115,** 2707–2718.

Holets, S., 1990: *Extreme Wind Speed Estimates in Northern and Central California.* Meteorology Services, Pacific Gas and Electric Company, 47 pp. plus appendixes. [Available from Meteorology Services, Pacific Gas and Electric Company, 77 Beale Street, San Francisco, CA.]

Holton, J. R., 1979: *An Introduction to Dynamic Meteorology.* 2d ed. Academic Press, 391 pp.

Idso, S. B., R. S. Ingram, and J. M. Pritchard, 1972: An American haboob. *Bull. Amer. Meteor. Soc.,* **53,** 930–935.

Kapela, A. F., P. W. Leftwich, and R. Van Ess, 1995: Forecast-

ing the impacts of strong wintertime post-cold front winds in the Northern Plains. *Wea. Forecasting,* **10,** 229–244.

Keyser, D., and M. A. Shapiro, 1986: A review of the structure and dynamics of upper-level frontal zones. *Mon. Wea. Rev.,* **114,** 452–499.

Liou, C.-S., R. M. Hodur, and R. H. Langland, 1994: Navy Operational Regional Atmospheric Prediction System (NORAPS): A triple nest mesoscale model. Preprints, *10th Conf. on Numerical Weather Prediction,* Portland, OR, Amer. Meteor. Soc., 423–435.

Nakata, J. K., H. G. Wilshire, and C. G. Barnes, 1981: Origin of Mojave Desert dust storms photographed from space on January 1, 1973. *Desert Dust: Origin, Characteristics, and Effect on Man,* T. L. Péwé, Ed., Geological Society of America, 223–232.

Nickling, W. G., and A. J. Brazel, 1984: Temporal and spatial characteristics of Arizona dust storms (1965–1980). *J. Climatol.,* **4,** 645–660.

Orgill, M. M., and G. A. Sehmel, 1976: Frequency and diurnal variation of dust storms in the contiguous U.S.A. *Atmos. Environ.,* **10,** 813–825.

Parkinson, G. R., 1936: Dust storms over the Great Plains: Their causes and forecasting. *Bull. Amer. Meteor. Soc.,* **17,** 127–135.

Pollard, M. C., 1978: Guidelines for forecasting dust storms in the southern Great Plains. *Natl. Wea. Dig.,* **3**(4), 40–44.

Shapiro, R., 1970: Smoothing, filtering, and boundary effects. *Rev. Geophys. Space Phys.,* **8,** 359–387.

Spaete, P., D. R. Johnson, and T. K. Schaak, 1994: Stratospheric-tropospheric mass exchange during the Presidents' Day Storm. *Mon. Wea. Rev.,* **122,** 424–439.

State of California, 1992: Dust-related collisions: Interstate 5, Panoche Junction Overcrossing/Kamm Ave. Task Force Report to Governor Pete Wilson, State of California, Business, Transportation, and Housing Agency, 99 pp. plus appendixes. [Available from the State of California, Department of Transportation, District 6, 1352 W. Olive Avenue, P.O. Box 12616, Fresno, CA 93778.]

Uccellini, L. W., 1990: Processes contributing to the rapid development of extratropical cyclones. *Extratropical Cyclones: The Erik Palmén Memorial Volume,* C. W. Newton and E. O. Holopainen, Eds., Amer. Meteor. Soc., 81–105.

Wilshire, H. G., J. K. Nakata, and B. Hallet, 1981: Field observations of the December 1977 wind storm, San Joaquin Valley, California. *Desert Dust: Origin, Characteristics, and Effect on Man,* T. L. Péwé, Ed., Geological Society of America, 233–251.

World Meteorological Organization, 1986: Atmospheric ozone 1985: Global ozone research and monitoring report. Rep. 16, WMO, 392 pp.

——, 1988: Manual on codes. Volume 1: International codes. Part A: Alphanumeric codes. WMO Publ. 306, 245 pp. plus appendixes. [Available from World Meteorological Organization, Casa Postale no. 5, CH 1211, Geneva 20, Switzerland.]